INTERNATIONAL ATOMIC ENERGY AGENCY
UNITED NATIONS EDUCATIONAL, SCIENTIFIC AND CULTURAL ORGANIZATION

INTERNATIONAL CENTRE FOR THEORETICAL PHYSICS
34100 TRIESTE (ITALY) - P.O.B. 586 - MIRAMARE - STRADA COSTIERA 11 - TELEPHONE: 2240-1
CABLE: CENTRATOM - TELEX 460392-1

H4.SMR.203 - 34

" SPRING COLLEGE ON GEOMAGNETISM AND AERONOMY "

(2 - 27 March 1987)

" Studies of the ionosphere through airglow "

presented by :

J.H.A. SOBRAL
Colegio Universitario de Humacao
University of Puerto Rico
C U H Station, Department of Physics
Humacao, Puerto Rico 00661
U.S.A.

INTERNATIONAL CENTER FOR THEORETICAL PHYSICS (ICTP) SPRING COLLEGE ON GEOMAGNETISM AND AERONOMY TRIESTE, ITALY 2-27 MARCH 1987

Lectures On "Studies Of The Ionosphere Through Airglow"
23-27 March 1987

by
J.H.A. Sobral

Colegio Universitario de Humacao
University of Puerto Rico
CUH Station, Department of Physics
Humacao, Puerto Rico 00661, USA

Table of Contents

		Page
1.	Abstract	3
2.	Introduction	6
3.	Brief Notes on the Terminology	9
	3.1 Airglow, Nightglow and Dayglow	9
	3.2 Emission Wavelength	10
	3.3 Zenith Direction	10
	3.4 The Ionosphere	10
	3.5 The Rayleigh Unit	12
4.	Basic Instrumental Components	13
	4.1 Introduction	13
	4.2 The Tilting Filter	13
	4.3 The Photo Multiplier Tube	15
	4.4 The Fabry-Perot Interferometer	15
5.	The Red (λ=6300 Å) and Green (λ=5577 Å) Oxygen Nightglows	17
	5.1 Introduction	17
	5.2 Theory of the OI 6300 Å Nightglow Generation	19
	5.3 Theory of the OI 5577 Å Nightglow Generation	27
	5.3.1 Introduction	27
	5.3.2 The F-region OI 5577 Å Nightglow	29
	5.3.3 The E region OI 5577 Å Nightglow	29
6.	The Low-Latitude Airglow	31
	6.1 Introduction	31
	6.2 The Ionospheric "Plasma Bubbles"	33
	6.3 Other Low Latitude Phenomena Studied Through Airglow	37
7.	The Mid-Latitude Airglow	40

8.	The High-Latitude Airglow	42
9.	All-Latitudes Airglow Studies	44
10.	The Geocoronal Airglow	45
11.	Ionospheric Studies through Man-Made Airglow	46
	11.1 Introduction	46
	11.2 HF-Heating-Induced Airglow	47
	11.3 Chemical Release Induced Airglow	49
12.	The Dayglow	50
13.	Perspective Optical Studies of the Ionosphere in the Near Future	52
	References	54

1. Abstract

This manuscript has been prepared to provide supplementary source of information for the 4-lecture course conducted by myself entitled "Studies of the Ionosphere Through Airglow", offered by the International Center for Theoretical Physics (ICTP) from March 23 to March 26, 1987 at the ICTP Trieste Headquarters in Italy. This course composes the ICTP sponsored "Spring College of Geomagnetism and Acronomy", all of it held in Trieste, Italy, during the period of March 2 to March 27, 1987. Several other courses composed the Spring College cited above. Namely, they were the following ones with their respective lecturers' names in parenthesis: 1) Main Magnetic Field, Secular Variations and Reversals (5 lectures, Dr. J.A. Jacobs, U.K.); 2) Geomagnetic Field Models, Current Systems in the Ionosphere (5 lectures, Dr. N. Fukushima, Japan); 3) Magnetospheric Processes (5 lectures, Dr. J.G. Roederer, USA); 4) Hydromagnetic Waves-Theory and Experiments (4 lectures, Dr. L.J. Lanzerotti, USA); 5) Radiowave Propagation (5 lectures, Dr. J.A. Klobuchar, USA); 6) Signal Processing and Time Series analysis (5 lectures, Dr. P. Fougere, USA);

7) Interplanetary Medium (3 lectures, Dr. F. Mariani, Italy); 8) Indices of Geomagnetic Activity and Features of Low Latitude Geomagnetic Field (4 lectures, Dr. C.K. Rangarajan, India); 9) Electromagnetic Induction Studies (4 lectures, Dr. B.P. Singh, India); 10) Radar Studies of the Ionosphere (4 lectures, Dr. R.F. Woodman, Peru); 11) The South Atlantic Magnetic Anomaly (4 lectures, Dr. S.M. Radicella, Argentina); 12) Features of the Equatorial Ionosphere (5 lectures, Dr. R.G. Rastogi, India); 13) Geomagnetic Disturbances at High Latitudes and Antarctic Research (4 lectures, Dr. A.N. Zaitzev, USSR) and 14) Planetary Ionospheres (2 lectures, Dr. S.F. Bauer, Austria).

Because many of those 14 courses just cited include topics on ionospheric physics, the present course will cover just a background material on ionospheric physics necessary to introduce the optical techniques used in ionospheric studies. Aurorae and airglow are the names for the upper atmospheric optical visible (red, green, yellow, etc.) and invisible (UV, EUV) light emissions. Several recent aurorae and airglow lines measurements and their implications in the studies of the ionosphere are reviewed. Also, a diversified number of ground-based, airborne,

satellite-borne and rocket-borne ionosphere and thermosphere physical and chemical studies are introduced with illustrations. Man-made aurora and airglow alterations are briefly discussed. The list of references found at the end of this work, is far from containing all relevant works in the field of study here concerned. It is both in numerical and alphabetical order. The use of bibliographical references represented by numbers within the text has the purpose of helping to shorten typescript spaces. However, authors names were used in the text whenever found appropriate.

2. Introduction

The optical techniques became so important for the studies of the ionospheric regions in the past 40 years that they formed unique ionospheric studies approaches which are conceptually different from the earlier techniques, namely, the ionospheric radiowave sounding techniques which have been profusely used since the first decades of the XX century. Both optical and radiowave techniques are very important diagnostic tools for ionospheric research and they often opportunely complement each other. In other words, there are classes of optical measurements that convey scientific information that is hardly obtained by any of the existing radiowave techniques and vice-versa.

The earth's upper atmosphere environment houses excited particles that are able to emit photons. Several particle species (O, H, N_2, etc...) emit light in a wide range of wavelengths. Generally speaking, there are two distinguishable categories of upper atmospheric emissions in the height range that goes from the basis of the thermosphere (approximately 80Km during nighttime) up to protonospheric heights (~600Km). One of them is called aurora and the other one is called airglow.

The former is generally caused by particle impact excitation of thermospheric constituents and typically occur at high latitudes while the latter are usually much weaker emissions caused by chemical reactions of thermospheric constituents. Both of them exist not only in the nightside but also in the sunlit side of the earth's upper atmosphere.

The airglow is usually a light of very weak brighthness so that it is rarely detected by the human eye. The aurorae lights are typically stronger than those of the airglow and are popularly known for their dramatic all-sky brightly colorful human-eye-detectable looks that typically occur at high latitude regions during energetic geomagnetic-field-aligned precipitation of charged particles into the high latitude ionosphere.

The history of the aurora science is chronologically different from that of the airglow. As it may be expected the former, because of the eye-visible high brightness of their events, were observed earlier. Historical records reveal aurorae observations as early as in the third, fourth and fifth centuries B.C. by ancient Greece observers such as, for example, Anaximenes (~550 B.C.) Anaxagoras (~450 B.C.) and Aristotle (~350 B.C.).

Airglow observations, on the other hand, started much more recently, namely, in the XX century. For further details on the hystory of the aurorae and airglow see, for example, the interesting hystorical review on that specific matter made by Chapman (1967).

The optical instruments regularly used in airglow intensity measurements are called photometers. They widely vary in size, geometry and engineering concepts depending upon the desired precision constraints, the space availability limitations as imposed by the type of carrier utilized (ground-based, rocket, aircraft, satellite, space shuttle) or other reasons. Modern concepts of imagers can perform digital and analog optical pictures of the sky at given airglow wavelenghts. A few samples of slide pictures will be displayed during this course. Optical techniques permit not only to measure airglow intensities, but also to measure other extremely important thermospheric parameters such as thermospheric neutral winds and temperatures. A brief description of the optical instrument that can perform such measurements, the Fabry-Perot interferometer, will be given later.

Here we have chosen to study the naturally occurring nighttime aurorae and airglow according to their spatial

distribution around the globe or, more specifically, according to their latitudinal range location. They are: the low, the mid and the high latitude regions. Typical natural nighttime phenomena that occur in those regions and that can be uniquely studied by means of optical techniques are, for example: 1st) at low latitudes: the ionospheric plasma bubbles and the equatorial Appleton Anomaly; 2nd) at mid latitudes: the stable auroral Red arc (SAR-arc); 3rd) at high latitudes: the ionospheric currents induced by the magnetosphere-ionosphere system.

Non-naturally, that is, man-made airglow, is here studied separately as a different category of airglow because their artifical triggering mechanisms introduce chemical behaviors that are inexistant in the naturally occurring photoemissive phenomena.

Further, the dayside emissions are briefly reviewed as well.

3. Brief Notes on the Terminology

3.1 Airglow, Nightglow and Dayglow

Airglow is the generic name given for the faint atmospheric emissions that stem from upper atmospheric regions. Some authors, however, prefer to call it either dayglow and nightglow depending whether it occurs in the

dayside (sunlit) or in the nightside, respectively. All of them are perfectly acceptable terminologies.

3.2 Emission Wavelength

Atmospheric emissions, whether auroral or airglow, are usually identified by their wavelength and not by their frequency. It is apparent that the Ångstrom (Å) or 10^{-12}m is more widely used. However, some authors prefer to use the nm (10^{-9}m) unit instead.

3.3 Zenith Direction

The zenith direction is the one that points vertically away from the earth.

3.4 The Ionosphere

The ionosphere can be roughly defined as the region of the earth's upper atmosphere where free electrons and ions are found in quantities sufficient to cause measurable effects on electromagnetic radiowaves (Rishbeth, 1969). Those ions and electrons form the ionospheric plasma. The type of ions found in the ionospheric domains depend on the height. The neutral atmosphere that coexists in space and in time with the ionosphere is denominated "Thermosphere" after its high thermal conductivity.

Typical ionospheric electron density height profiles are shown in Fig. 1. The electron density

vertical structures permit to divide the ionospheric regions as follows: 1) The D-region (50-90Km); 2) the E-region (90-150Km); 3) the F-region (150-600Km) and 4) protonosphere (~600Km upwards). The height ranges shown in parentheses are just approximate values since they largerly vary with time, season and geographic location.

The D-region characteristically appear during daytime and causes typical radiowave absorptions in the HF band. The E-region is also called the "dynamo region" because it is the source of polarization electric fields which, in turn, play extremely important roles on the dynamics of the ionospheric plasma. Typically, as at low latitudes, those electric fields can eventually get mapped from the E-region into the F-region, through the highly conducting geomagnetic field lines causing F-region plasma motions (drifts).

The F-region is the most dense and from many points of view, the most important part of the ionosphere. Its plasma is dominated by atomic oxygen atoms and electrons. Its maximum electron density (NMAX) is very often referred to as the F-region peak and its height is denoted by HMAX. The F-region dynamics is strongly affected by a wide variety of causes such as neutral winds,

tides, electric fields, etc... During daytime the F-region may appear divided into two layers separated by a couple of tens of kilometers from each other. Those layers are the F1 (lower height) and the F2 (upper height) layers.

Much of the airglow emissions relevant to ionospheric studies stem from the F-region.

In the F-region, both electrons and ions spiral around the geomagnetic field lines which makes those lines particularly highly electrically conductive. Such charged particles binding to the geomagnetic field lines explains the very commonly observed bulk field aligned motions of the ionospheric F-region plasma.

Finally, the Protonosphere follows in altitude, the F-region and it is mostly constitued by hydrogen ions (H^+).

For detailed information about the ionospheric regions the reader is suggested to refer to Rishbeth (1969).

3.5 The Rayleigh unit

Because the airglow emissions are very faint lights, a convenient unit, namely, the Rayleigh, has been established. One Rayleigh equals 10^6 photons cm^{-3} Sec^{-1} sr.

4. Basic Instrumental Components

4.1 Introduction

A few details on the interference filter, which is extensively used in airglow measurements, will be given below. The Fabry-Perot optical interferometer system will be also described.

4.2 The Tilting Filter

The tilting filter is an optical device composed of light-transparent plates separated by a very small distance. Between those two plates light gets reflected a number of times and the reflected rays interfere with each other in such a way that only certain wavelenghts will pass through the filter (see Bather and Reasoner, 1969). The transmitted wavelength varies with the initial angle of incidence so that for each incidence angle of the nonmonochromatic light, different wavelength bands will pass.

The transmittance of the filter is the ratio of the light intensity before and after passing through the filter. For parallel incident light (i.e., light from a distant point source) the peak of the transmittance is shifted to smaller wavelenghts as the angle of incidence moves from its perpendicular as shown in Fig. 2 (source:

Wickwar, 1971). Analogous shifts happen to conic incidences. A comparison between parallel and conic incidences is shown in Figs. 2 and 3. Notice the constant amplitude transmission peaks for the parallel incidence angle opposed to the decreasing towards lower wavelengths transmission peaks for conic incidence. The conic incidence allows a sharp discrimination of the 6300 Å wavelength as characterized in Fig. 3 by spreading and flatening the transmission band pass at neighboring wavelengths.

Similar effects arise from temperature variations. An increase of temperature results in an increase of the wavelength of the peak transmission.

The interference filter is made to rotate around its diameter during airglow experiments, in order to adequately let pass the desired wavelength. That is the reason why this type of filter is also referred to in literature as "rocking" or "tilting" filter. The resulting signal is illustrated in Fig. 4 where the lowest signal levels represent background noise which is composed of a mixture of signals from sources like stars, atmospheric emissions and instrumental noise. The distance from the signal peak to the background level is the measurement to

be obtained from those records and it is proportional to the OI 6300 Å airglow intensity (in this illustration the airglow wavelength being measured is 6300 Å).

4.3 The Photomultiplier tube (PMT)

Certainly, the very faint filter-transmitted airglow line discussed in the previous section has to be transformed into some sort of instrumentally measurable signal. Photomultiplier tubes are used for that purpose. Figure 5 (source: Wickwar, 1971) shows a typical photomultiplier tube housing installation. The lens shown in the left hand side converges the incoming light into a conic light beam that is focused at the PMT input. The PMT output electrical signal, of course, has to be greatly amplified. Fig. 6 (source: Wickwar, 1971) shows a schematic diagram of the electronic circuit that follows the PMT.

Fig. 7 (source: Anger, 1967) shows the scheme of an auroral scanner assembly used in photometric rocket experiments. Notice the similarity of the rocket-borne and ground-based photometric basic systems, as shown in Figs. 5 and 6.

4.4 The Fabry-Perot Interferometer (FPI)

The Fabry Perot interferometer is presently a very

important technique that can provide both temperature and wind measurements of the nighttime F-region neutral species. The importance of the FPI these days is mostly due to the fact that it is the only ground-based instrument capable of measuring the F-region neutral winds and temperatures. Those measurements are normallly very important for the study of the dynamics of the ionospheric plasma, including its interactions with the neutral atmosphere (thermosphere). The name Fabry-Perot came after its inventors, French optician Charles Fabry (1867-1945) and his colleague co-worker A. Perot.

Two plate devices transparent to light form the so-called Fabry-Perot "étalon". Phase changes caused by reflected light interactions between those two devices give rise to the typical Fabry-Perot concentric dark and bright circular fringes that are projectable in a plane parallel to the etalon. Details on the mathematical analysis of the Fabry-Perot interferometric properties are given by Hernandez (1966) and references therein.

Fig. 8 shows a schematic diagram of a Fabry-Perot System (source: Biondi, personal communication, 1987).

Fig. 9(c) shows a sketch of a ground-based FPI set-up for measuring the 6300 Å emission that stems from

ionospheric F-region atomic oxygen (OI 6300 Å). Figs. 9b and 9a shows typical FPI bell-shapped intensity versus wavelength outputs. Velocity changes of the emitting atomic oxygen atoms population, in the direction of the line of sight, causes parallel Doppler shifts in the curve (Fig. 9b). Temperature increases in the ionospheric F-region atomic oxygen atom populations cause spectral widenings as depicted in Fig. 9a.

5. The Red (λ = 6300 Å) and the Green (λ = 5577 Å) Oxygen Nightglows

5.1 Introduction

Red (λ = 6300 Å) and green (λ = 5577 Å) airglow is widely produced by excited ionospheric oxygen atoms everywhere in the night side of the earth globe. In particular, the atomic oxygen red airglow is about the most extensively used airglow in the study of the dynamics of the nighttime ionospheric F-region. It arises from an emitting layer approximately 50Km thick located just below the F-region peak. The red airglow intensity increases or decreases as the ionospheric plasma moves downwards or upwards respectively, as we shall see later with more detail. Consequently, airglow variations can be used to study nighttime vertical motions (drifts) of the

ionosphere. The intensity of such airglow gets more or less intense as the ionospheric electron density is larger or lower, respectively. In that way, the low latitude ionospheric bubbles, which are field-aligned highly depleted regions of the nighttime ionospheric plasma, have been extensively studied by means of the atomic oxygen red line airglow, resulting in significant improvements in the understanding of that particular nighttime ionospheric phenomena (see for example references no. 65, 66, 71, 72, 73, 74, 80, 82, 83).

As mentioned earlier, the ionospheric red airglow has been also extensively used to measure ionospheric neutral winds resulting in valuable contributions to the understanding of the interactions between the ionospheric plasma and the ambient neutral atmosphere (48 and references therein).

On the other hand the green atomic oxygen nightglow, although generally not as frequently used in ionospheric studies as the red airglow, has brought also important advances to the knowledge of the nighttime ionospheric plasma dynamics. It stems both from the E and F ionospheric regions and has been used to study neutral

atmospheric perturbations at the ionospheric E-region heights (7. 13, 31, 60, 67, 68, 75, 76, 84).

The photoemissive electronic orbital transitions of the oxygen atom (OI) are depected in Fig. 10.

Following, the theories for the red and the green line airglow will be reviewed.

5.2 Theory of the OI 6300 Å Nightglow Generation

Detailed theoretical studies on the OI 6300 Å generation have been extensively made by Peterson et al (1969) Peterson (1966) and Peterson et al (1968). Wickwar (1971) presented a comprehensive description of the OI 6300 Å production mechanisms similar to the one to be developed here. More recently, Cogger (1980) has established a new expression for the OI 6300 Å volume emission rate adopting up-to-date laboratory measurements of reaction rates.

Photoemissive electron orbital transitions in the oxygen atom produces visible light (Fig. 10). The electron orbital transition concerned in this section is the $^1D_2 \rightarrow {}^3P_2$ transition, which is followed by the emission of a 6300 Å photon.

Chemical reactions in the nighttime ionosphere produce metastable oxygen atoms at energy levels up to the

^1S_o level. The photoemission at λ = 6300 Å at night takes place almost entirely in the F-region.

The dissociative recombination of molecular oxygen ions in the ionosphere is the main metastable oxygen atoms production mechanism.

The following set of reactions describes the dissociative recombination production of metastable oxygen atoms in the nighttime ionospheric F-region:

$$O^+ + O_2 \rightarrow O_2^+ + O + 1.53eV \quad \gamma_1 \qquad 5.2.1$$

$$O_2^+ + e \rightarrow O + O + 6.96\,eV \quad \alpha_1 \qquad 5.2.2$$

where γ_1, and α_1 are reaction rates and e stands for electron.

The ion-atom interchange reaction 5.2.1 produces 1.53 eV of extra energy.

The 6.96ev energy available resulting from the reaction 5.2.2 may be partially absorbed by the two oxygen atoms resulting, consequently, in metastable oxygen atoms. Branching ratios of about 1.0; .9; .1 for the production of $O(^3P)$, $O(^1D)$ and $O(^1S)$ respectively, is expected from reaction 5.2.2. The dissociative recombination of NO^+ was formely believed to be the second main source of $O(^1D)$'s by means of the reactions shown below:

$$O^+ + N \rightarrow NO^+ + 1.09\ eV \qquad \gamma_2 \qquad 5.2.3$$

$$NO^+ + e \rightarrow N + O + 2.76\ eV \qquad \alpha_2 \qquad 5.2.4$$

where γ_2 and α_2 are reaction rates. However, such a source has been shown later on to be improbable because of the lack of spin conservation.

Therefore reactions 5.2.1 and 5.2.2 account for practially the totality of the $O(^1D)$ atoms production in the nighttime F-region.

The $O(^1D)$ atoms eventually can get quenched (de-excited) in the F-region either by natural electron orbital transition with subsequent emission of light or by collisions with ambient neutral particles.

Quenching by electrons, O and O_2 is generally assumed to be negligible.

According to reaction 5.2.2 we can write the following time-dependent differential equation:

$$\frac{d}{dt}[O(^1D)] = R\alpha_1[e][O_2^+] \quad cm^3\,sec^{-1} \qquad 5.2.5$$

where [ ] denotes particle concentration and R denotes the average number or $O(^1D)$'s produced per recombination of O_2

including cascading from the ^1S state.

Accordingly, from reaction 5.2.1 we can write:

$$\frac{d}{dt}[O_2^+] = \gamma_1[O_2][O^+] \quad cm^3\,sec^{-1} \qquad 5.2.6$$

The O_2^+ continuity equation gives us:

$$\frac{d}{dt}[O_2^+] = \gamma_1[O_2][O^+] - \alpha_1[e][O_2^+] - div\{[O_2^+]V_{O_2^+}\} \qquad 5.2.7$$

where $V_{O_2^+}$ is the average O_2^+ velocity in the unit volume considered.

Peterson et al (1966) have shown that both the divergence and the time derivatives terms of equation 5.2.7 are negliglible with respect to the other terms of that equation. Therefore, we can write:

$$\gamma_1[O_2][O^+] = \alpha_1[e][O^+] \quad cm^3\,sec^{-1} \qquad 5.2.8$$

Substituting 5.2.8 in 5.2.5 we obtain:

$$\frac{d}{dt}[O(^1D)] = R\gamma_1[O_2][O_2^+] \quad cm^3\,sec^{-1} \qquad 5.2.9$$

The time derivative term of the expression 5.2.9 is the de-excitation rate of the $O(^1D)$ due to all possible photoemissive electron orbital transitions of the $O(^1D)$ atom.

The $O(^1D)$ quenching by collisions with N_2

molecules occurs according to the following reaction:

$$N_2 + O(^1D) \rightarrow N_2 + O(^3P) \qquad Q \qquad 5.2.10$$

where Q is the quenching coefficient. Thus, according to the reaction 5.2.10 the rate of de-excitation of $O(^1D)$ atoms due to collisions with N_2 molcules is given by:

$$\frac{d}{dt}\left[O(^1D) \rightarrow O(^3P)\right] = Q\,[O(^1D)][N_2] \qquad 5.2.11$$

Considering natural quenching (de-excitation followed by emission of light) only, the de-excitation rate of the $O(^1D)$ is given by:

$$\frac{d}{dt}\left[O(^1D) \rightarrow O(^3P)\right] = A_{6300}\,[O(^1D)] \qquad 5.2.12$$

where $\mathring{A}_{6300}$ is the Einstein coefficient for the 6300 A transition. Considering now all possibilities of both orbital transitional and collisional de-excitation equation 5.2.12 becomes:

$$\frac{d}{dt}\left[O(^1D) \rightarrow O(^3P)\right] = A_{6364}[O(^1D)] + A_{6392}[O(^1D)] + A_{6300}[O(^1D)] + [N_2][O(^1D)] \qquad 5.2.13$$

The probability P(6300 A) that an $O(^1D)$ atom will emit a 6300 $\mathring{A}$ photon is given by:

$$P(6300\,\mathring{A}) = \frac{A_{6300}}{A + Q[N_2]} \qquad 5.2.14$$

where $A = A_{6300} + A_{6392} + A_{6364}$.

From expressions 5.2.14 and 5.2.9 the 6300 A emission rate is given by:

$$\frac{d}{dt}\left[O(^1D) \rightarrow 6300\,\mathring{A}\right] = \frac{A_{6300}}{A + Q[N_2]}\, R\gamma_1[O_2][O^+] \qquad 5.2.15$$

photons $cm^{-3}\,sec^{-1}$

Peterson et al (1966) using the nighttime continuity equation found the the ratio F defined as:

$$F = \frac{[O^+]}{[e]} = \frac{1}{1 + \frac{\beta_1[O_2]}{\alpha_1[e]} + \frac{\beta_2[N_2]}{\alpha_2[e]}} \cong 1 \qquad 5.2.16$$

Substituting 5.2.16 into 5.2.15 and integrating from the thermospheric base height h_1 to some adequately chosen F-region top level h_2 results:

$$I_{6300} = \int_{h_1}^{h_2} \frac{dh\; A_{6300}}{A + Q[N_2]}\, R\gamma_1[O_2][e] \quad \text{photons } cm^{-2}\,sec^{-1} \qquad 5.2.17$$

where I_{6300} stands for the OI 6300 A emission intensity.

The I_{6300} can be expressed in Rayleighs as:

$$I_{6300} = 10^{-1} \int_{h_1}^{h_2} \frac{A_{6300}}{A + Q[N_2]} \gamma_1 R [O_2][e] F \, dh \qquad 5.2.18$$

where R = .5, h is in Km, and the particle concentration in cm^{-3} units.

Figure 11 shows OI 6300 Å airglow emission profiles calculated by the author utilizing the expression 5.2.18.

On the other hand, in a more recent study cn the generation of the OI 6300 Å airglow, Cogger et al (1980) establishes the OI 6300 Å volume emission rate as:

$$\eta_1 = .76\, \varepsilon_1 k_3 [O^+][O_2] D_1 F_1$$

where ε_1 =1.3 (adimensional) and

$$D_1 = \frac{1 + k_2[N_2]}{A_{6300} + A_{6364}}$$

where k_2 and k_3 are, respectively, the collisional de-excitation rates of the $O(^1D)$ atoms (note: we have previously represented the K_2 rate by the letter Q) and the ion-atom interchange reaction (former, γ_1).

The terms F_1 and B are given by:

$$F_1 = \left[\frac{1 + K_4[N]}{\alpha_1[e]}\right]^{-1}$$

$$B = \frac{[O^+]}{[e]}$$

and assuming three-ion F-region ionospheric composition:

$$[e] = [O^+] + [O_2^+] + [NO^+]$$

$$[e] = [O^+]\left[1 + \frac{K_3[O_2]}{\alpha_1[e] + k_4[N]}\left[1 + \frac{K_4[N]}{\alpha_9[e]}\right] + \frac{k_{10}[e]}{\alpha_9[e]}\right]$$

where α_1 , k_4, k_9 and k_{10} are rates for the following reactions:

$$O_2^+ + e \rightarrow O + O \quad \ldots \alpha_1$$
$$O_2^+ + N \rightarrow NO^+ + O \quad \ldots k_4$$
$$NO^+ + e \rightarrow N + O \quad \ldots \alpha_9$$
$$O^+ + N_2 \rightarrow NO^+ + N \quad \ldots k_{10}$$

In his calculations, Cogger (1980) has assumed certain conditions, that we havent't considered in our previous derivations, such as for example $B \neq 1$ and the three last reactions indicated above.

Sometimes it is rather convenient to see the I_{6300} as resulting from its main terms that is:

$$I_{6300} \propto \int_{h_1}^{h_2} \frac{[O_2][e]}{[N_2]} \, dh \qquad 5.2.19$$

Through expression 5.2.9 it becomes easier to verify the airglow intensity changes due to changes of ionospheric height. When the nighttime ionospheric F-layer descends, I_{6300} tends to increase in amplitude because of the exponentially increasing atmospheric O_2 concentration. At the same time I_{6300} tends to decrease due to the exponentially increasing N_2 concentration. The final

result is that I_{6300} increases with the ionospheric layer descent because the ratio $[O_2][e]/[N_2]$ tends to increase as the ionosphere descends. So, the increase (decrease) of the OI 6300 Å as the ionosphere descends (ascends), becomes a fundamental rule that can be practically always trusted. Notice, however, that the opposite is not true. For example, assume that the ionospheric plasma will not move vertically. So we can consider now that the $[O_2]/[N_2]$ ratio remains constant with time. Assume now that for some reason e decreases (increases). Then according to the expression 5.2.19 I_{6300} will decrease (increase). The former case explains the big airglow depletions observed during the occurrence of low-latitude ionosphere plasma bubbles (or plasma depleted regions) that we shall see later in the studies of the low latitude ionosphere dynamics. Therefore, OI 6300 Å nightglow intensity variations may not be straightly interpretable, that is, it may not be possible to pinpoint its cause just by inspecting the airglow intensity variations.

5.3 Theory of the OI 5577 Å Nightglow

5.3.1 Introduction

As depicted in Fig. 10 the OI 5577 Å (green) emission results from the $O(^1S_o) \rightarrow O(^1D_2)$ photoemissive

electron orbital transition. The atomic oxygen atom excitation to the ^1S_o state takes place in the nighttime E and F regions via different excitation mechanisms. In the former region the $O(^1S_o)$ population arise from three body collision reactions envolving neutral species only. Therefore such an emission conveys information on the dynamical status of the neutral atmosphere. In the F region $O(^1S_o)$ atoms result from the same dissociative recombination process described in the last section, that is, via the same mechanism that generates the red airglow. Therefore, the F-region-produced OI 5577 Å nightglow conveys little information on upper atmospheric dynamical conditions except for the fact that when it is subtracted from the OI 5577 Å nightglow observed from ground it results in the net E-region produced OI 5577 Å nightglow which is actually a rather important information. In fact, the ionospheric F-region OI 6300 Å nightglow, as observed from ground, conveys all the useful ionospheric plasma information that the ground observed OI 5577 Å airglow can possibly convey with the advantage of not having the complications introduced by the contamination of the E-region OI 5577Å nightglow.

It seems that the E-region OI 5577 Å nightglow has not been as widely used for ionospheric studies as the OI 6300 Å nightglow. However, the former airglow may provide unique information on the neutral atmosphere in a height range where data on the neutral atmosphere is not very easily achieved by the current experimental techniques, since that height range is too low for satellite orbits and too high for balloon experiments. Rockets can certainly go through it but they are very costly and get data for just small amounts of time, so that it gets severe usage limitations. Hernandez and Turtle (1967) were able to measure E-region temperatures by means of Fabry-Perot ground measurements of the OI 5577 Å nightglow. Sobral (1979) and Gadsden and Marovich (1969) detected OI 5577 Å variations caused by disturbances on the neutral atmosphere at E-region heights. Dandekar and Turtle (1971) carried out atomic oxygen concentrations in the E-region utilizing OI 5577 Å airglow intensity data.

Following, we shall briefly see the OI 5577 Å emission generation mechanisms.

5.3.2 The F-region OI 5577 Å nightglow:

As generated by the dissociative recombination process described in detail in section 5.2 the F-region

OI 5577 Å intensity, I_{F5577}, can be easily shown to be given by:

$$I_{5577} = 10^{-1} \int_{h_1}^{h_2} \frac{A_{6300}}{A} \gamma_1 R [O_2][e] F \, dh \qquad 5.3.1$$

where R = .05.

Fig. 12 shows E-region OI 5577 Å nightglow intensities obtained by the author, by subtracting the F-region intensity as given by the expression 5.3.1 from the total OI 5577 Å airglow intensity observed from ground at Arecibo, Puerto Rico.

5.3.3 The E-region OI 5577 A Nightglow:

The so-called Chapman mechanism predicts the E-region production of the $O(^1D)$ atoms through the following reactions:

$$O + O + O \rightarrow O_2 + O(^1S) \qquad \delta_1$$
$$O(^1S) \rightarrow O(^1D) + h\nu_{6577} \qquad A_{5577} = 1.28\ sec^{-1}$$
$$O(^1S) \rightarrow O(^3P) + h\nu_{2972} \qquad A_{2972} = .078\ sec^{-1}$$
$$O(^1S) + O_2 \rightarrow O_2 + O \qquad \delta_2$$
$$O(^1S) + O \rightarrow O + O \qquad \delta_3$$

where the A's represent the Einstein's coefficients and δ_1, δ_2 and δ_3 represent reaction rates.

The E-region OI 5577 Å emission intensity, I_{E5577}, can be shown to be given by:

$$I_{5577_E} = 1.28 \times 10^{-6} \int_0^{\infty} \frac{\delta_1[O]}{\delta_2[O_2] + \delta_3[O] + 1.36} dh$$

where 1.36 represents the sum $A_{5577} + A_{2972}$.

6. The low latitude Airglow

6.1 Introduction

Many airglow lines can be studied at low latitudes. However, in this section, attention will be focused on the OI 6300Å nightglow for two basic reasons. First because of natural size limitations on this work. An over-extended discussion here would make difficult to focus the present discussion on some particularly important ionospheric OI 6300 Å nightglow features at low latitudes. Second because perhaps the OI 6300Å nightglow has been more extensively used than any other airglow line during the last 20 years for studying the low latitude nighttime ionosphere.

It is well-known that the low-latitude and equatorial ionosphere suffer dramatic structural changes during nighttime, specially during equinoctial and summer postsunset period. Such changes occur within the volumen

of ionospheric highly plasma depleted regions that are currently referred to as the "ionospheric plasma bubbles".

Such denomination arises from the fact that wide and very long (geomagnetic field-aligned) bubble-like ion depleted regions physically define the ionospheric bubble volume contour.

The ionospheric bubble events are accompanied of very structured and turbulent plasma regime. One of the most puzzling findings in the field of radiowave communications in last decade was the fact that radiowaves with frequencies of the order of a couple of GH_z utilized in satellite communications were found to get severely affected by small structure ionospheric irregularities at low geomagnetic latitude. Surprisinglly, evidences show that such radiowave interferences with the ionospheric plasma can get even more intense than those that occur at high latitudes in the neighborhood of the auroral zone where intense ionospheric plasma turbulence regimen is often present. Consequently, the study of the ionospheric plasma bubbles at low and equatorial regions of the earth became a requirement to minimize the undesired electromagnetic interference effects of the turbulent-regime plasma bubbles with ground to satellite

telecommunications links. A better understanding of the electrodynamic inner structure of the ionospheric bubbles became of fundamental importance in oder to introduce the necessary polarization corrections on the communications satellite GH_z links.

Further, the bubble events became a notorious research topic for plasma physicists. The ionosphere unique size, composition and density structure is hardly reproduceable in laboratory. Ionosphere physicists and plasma physicists were able to develop theories to explain the complicated plasma instability generation mechanisms that give rise to the ionospheric bubbles.

OI 6300 Å nightglow studies have greatly helped to understand the plasma bubble physics by determining the bubble geometric extents and its progress with time.

A concise description of the ionospheric plasma bubbles studies performed utilizing the OI 6300 Å nightglow will follow. Subsequently, in this work, studies on the equatorial anomaly and low latitude particle precipitation will be given.

6.2 The Ionospheric Plasma Bubbles

As discussed in the last section the ionospheric plasma bubble phenomena became a topic of interest for

research and applied work in areas such as ionosphere physics, fundamental plasma physics, radiowave propagation and many other areas.

Theorists generally agree that the ionospheric plasma bubbles are triggered at the lower edge of the F-region, that is, below the F-region peak, by the Rayleigh-Taylor instability of the ionospheric plasma. It can be theoretically shown that sharp sub-peak vertical electron density gradients as well as large upwards velocities of the ionospheric plasma increase the plasma instability growth rate. Experimental data in fact confirm that sharp electron density gradients as well as enhanced upwards velocity on the ionospheric layer, actually occur during the moments preceding the commencement of plasma bubble events.

Ionospheric plasma bubbles can also be detected by ground-based radiowave diagnostic techniques. The bubbles typically cause both range-spread F and VHF intensity scintillations which, in turn, are detectable by means of ionosondes and polarimeters, respectively. Polarimeters also detect the plasma bubbles electron density depletions.

Fig. 13 sketchly shows the spatial extent of the ionospheric bubble. Fig. 12.a shows a typical east-west contour of the bubble, where the bubble "head" appears as an enlarged region on the top and the bubble "neck" appears as parallel lines at the bottom. Fig. 13.b approximately shows NS configuration of the bubble head.

The vertical evolution of the bubbles occur field-alinedly from lower altitudes to higher altitudes. However at the same time, the bubbles seem to be generated practically simultaneously over hundreds of kilometers along the geomagnetic field lines. The sketch shown in Fig. 13.b suggests then that the bottom bubble has started later than the upper bubble. Further, it can be verified from Fig. 13.b that as the bubble head rises, its footprints move polewards.

Fig. 13 (source: Sobral et al., 1981) shows a sequence of OI 6300 A nightglow magnetic meridional profiles obtained in Brazil (45°W 23°S) utilizing a scanning photometer that continuously scanned the vetical plane from 75° south of zenith to 75° north of zenith indicated in that figure. Strong airglow valleys are clearly seen in Fig. 13. They propagate from the right hand side to the left hand side and from the top to the

figure. Clearly, such features display a poleward propagation which in fact, represent the poleward bubble footprint propagation cited in the last paragraph.

The ionospheric bubbles can also be optically detected by means of airglow imagers. Weber et al (1982) obtained a large number of images utilizing an OI 6300 Å imager installed aboard an aircraft (Figs. 15 to 18; see a also references no. 50, 81, 82, 83 and 84). Their aircraft flight plans are shown in Fig. 19. The Weber et al's imager had a field of view of about 155° centered at zenith. The 2-dimensional images shown in Fig. 14 (Weber et al 1982) clearly show spatial structures of the bubble as evidenced in those images as dark strips diametrally ranging across the image. Notice the eastward movement of the bubble moreover, Weber et al's airborne measurements were made concurrently with AE-E satellite measurements of the atomic oxygen ion concentration (see Fig. 18). Figs. 16, 17 and 18 clearly show that the bubble dark signatures in the images correspond to depletions of the O^{+} concentration. Notice also in those figures that OI 7774 Å nightglow measurements have been performed as well. The OI 7774 Å nightglow primarily results from radiative reconbination of the atomic oxygen ion and its volume

emission rate is propotional to the square of the electron concentration. About 50% of the OI 7774 Å emission arises from above the F-region peak as opposed to the OI 6300 Å airglow that mostly stems from below the F_2-peak.

6.3 Other Low Latitude Phenomena Studied Through Airglow

General views of the low latitude airglow studies were given by Barbier (1957), Barbier (1958), Steiger (1967) and Weill (1967).

Magnetic storm effects and other ionospheric responses at low latitudes were computer modelled by Fesen and Abreu (1987).

The nighttime low-latitude Appleton anomaly causes the appearance of two zonally-aligned strips of enhanced OI 6300 Å emission. The strips are located in each side of the magnetic equator, at geomagnetic latitudes of approximately $\pm 15^{\circ}$. The strips are of the order of a few degrees of latitude wide and many degrees of longitude long (see Barbier, 1958).

The ionosphere dynamics has been extensively studied at Arecibo, which is a geographic-low-latitude station (18°N) but at the same time it is magnetically-mid-latitude station (50° dip).

Using OI 6300 Å and OI 5577 Å nightglow intensity data, Sobral et al (1978) studied several aspects of the ionospheric dynamics during nighttime over Arecibo, focusing attention on the ionospheric descent that usually occurs at that site around 24:00 LT. That descent has been generally quoted as the Arecibo "ionospheric midnight collapse" after its time of ocurrence.

Nelson and Cogger (1971) and Herrero and Meriwether (1981) also carried out studies on the ionosphere dynamics over Arecibo utilizing airglow data. Herrero and Meriwether (1981) used a ground-based OI 6300 A imager in their Arecibo nighttime thermospheric neutral-winds-field studies. Kerr et al. (1986) performed high resolution measurements of the geocoronal Balmer α ($H\alpha$) utilizing a Fabry-Perot interferometer. They studied the following specific aspects of the exosphere: 1) exospheric hydrogen concentrations, 2) exosphere temperatures, 3) exosphere evaporative cooling due to escape of thermalized hydrogen atoms, 4) exospheric velocities distribution and, finally, 5) the H α emission by multiply scattered solar Ly α radiation.

Tinsley et al 1986 (see also references therein) studied in detail the low-latitude aurorae that result from

energetic particles precipitation during ring current disturbance events. The spectral lines associated to the low latitude aurorae are shown in Table 2 (source: Tinsley et al, 1986). Tinsley et al's (1986) work show the history of the studies carried out during the last half century on the vibrational excitation of the first negative band of the molecular nitrogen ion (N_2^+1N) as created by energetic precipitation of oxygen, helium and either ion or neutral hydrogen. Tinsley et al. state that the low-latitude aurora is characterized by the following features: 1) N_2^+1N emission, 2) a high (>10) OI 6300 Å/OI 5577 Å airglow ratio and 3) prominence of atomic/ionic lines from O, O^+, N and N^+ as compared to molecular bands.

Highest low latitude aurora brightness levels are found at about 40° dip ltitude. Low latitude (0° - 40°) aurorae are caused by energetic neutral atom precipitation, which originate from charge of energetic ring current ions with exospheric hydrogen. About three independent mechanisms can account for the N_2^+1N excitation: 1) precipitation of heavy particles (ions or neutral atoms H, He, O); 2) sunlight resonant scattering through N_2X ions; 3) collision of large fluxes of low energy electrons with N_2X ions.

Table 1 shows a variety of low latitude aurorae wavelengths (source: Tinsley et al 1986).

7. <u>The Mid Latitude Airglow</u>

At mid-latitudes, the most striking airglow feature is that of the Stable Auroral Red Arc (SAR) (15, 16, 17, 32, 38, 41, 43 and 80). The SAR arcs are zonally-elongated thin (just a few degrees of latitude wide) and very long (possibly zonally circunscribing the whole earth (Tinsley et al 1986)) fringes of enhanced OI 6300 Å airglow. It is understood that the excitation of the atomic oxygen to the ^{1}D state (responsible for the SAR arcs 6300 Å emission) is caused by hot (3000-8000°K) ionospheric thermal electrons (Kozyra et al, 1982). The problem however regards the source mechanism for those thermal electrons. Several hypotheses for the source mechanism have been proposed. Cole (1965) proposed that plasmaspheric thermalized electrons can obtain energy through coulomb collisions with energetic ring current protons. Cornwall et al (1971) suggested that the interaction of ring current protons with cold plasmaspheric electrons produce ion-cyclotron waves that, in turn, are absorbed by the cold electrons via Landau damping. The energized electrons then flow downwards toward the ionosphere via the geomagnetic field

lines. More recently, Hazegawa and Mima (1978) suggested that the plasmaspheric electron energization may result from resonant interactions between plasmaspheric electrons and Alfven waves when those waves wavelength in the direction perpendicular to the magnetic field is comparable with the ion gyro radius.

Figure 20 displays a sketch on the SAR arc geometry. The SAR production of 6300 Å emission occur throughout height ranger (~250Km to 600Km) that are much larger than those that correspond to the dissociative recombination emissive layer (~250-450Km) previously discussed. Craven et al (1982) show clear satellite pictures of the SAR arcs.

Tinsley et al (1986) assert that from mid to high latitudes, that is, from about 40° dip latitute to the auroral zone, downward fluxes of energetic O^+, H^+ and He^+ may cause ionospheric airglow emissions through collisional excitation. Those airglow emissions of course are distinct from the red SAR emission.

Ishimoto and Torr (1986) review the role of energetic O^+ precipitation airglow effects at mid latitudes. Torr and Torr (1984) reported on observed ground-based effects of energetic oxygen atoms in the midlatitude aurora.

8. <u>The High-Latitude Airglow</u>

Because of the precipitation of energetic particles, specially the precipitation of energetic electrons, the auroral emission at high latitudes gets particularly intense. Table 2 displays several high-latitude emission lines as measured by satellite (source: Chakrabarti, 1986).

Frank and Craven's (1982) satellite Extreme-Ultra-Violete (EUV) images present for the first time a global picture of the theta-shaped aurora. In those pictures a remarkable theta-shaped luminosity appears. The luminosity arises from ionospheric atomic oxygen emissions at λ = 1304 Å and λ = 1356 Å. The bar in the middle of the theta-figure is sun-earth aligned. Each theta half form a current cell. Fig. 21 illustrates the theta-shaped aurora as seen in the satellite images just described.

Anger (1967) review rocket auroral measurements. Akasofu and Kan (1981) present the physics underlying the formation of the auroral arc.

Bythrow et al (1986) studied remotely distant plasma sheet boundary waves event as evidenced by auroral arcs luminosities and Birkeland (field-aligned) currents.

Erdman and Zipf (1986) carried out laboratory measurements of the excitation and quenching rates of the $N(^5S)$ resulting from dissociative excitation by electron impact on N_2. Gerard and Noel (1986) presented satellite contaminations by the $N^+(^5S)$ emissions.

Roach (1967) reviewed the worldwide auroral morphology. Thomas (1967) discussed the interpretation of ionospheric processes by means of aurora and airglow.

Studies on airglow from individual species have been made by Rees (1984, 1985) and by Myrabo et al (1986). Rees (1984) studied the excitation of the $O(^1S)$ and subsequent emission at λ = 5577 Å. Rees (1985) studied the atomic nitrogen optical emissions. Myrabo et al (1986) analysed mid-winter intensities of the high-latitude O_2(2-1) nightglow. Richards and Torr (1985) investigated the production of the N^+ at high-latitudes.

Peterherych et al (1985) studied vertical wind structures between two intense auroral arcs. McCoy (1983) performed NO, $N(^4S)$ and $O(^3P)$ densities measurements based on rocket measurements of the NO and O_2 airglow.
UV and EUV/satellite measurements at high latitude were reported by Charkrabarti (1985, 1986), Daniell and

Strickland (1986) and many other authors (see references contained in each of those works).

9. <u>All Latitudes Airglow Studies</u>

This section concerns airglow studies that have been made over extended latitudinal ranges during very long periods of time. There are just a few of those studies.

Roach and Smith (1967) reviewed the worldwide morphology of the atomic oxygen red (6300 Å) and green (5577 Å) airglow.

Fig. 22 shows the OI 6300 Å and the OI 5577 Å source regions as a function of magnetic latitude and height. Figure 23 shows the latitudinal distribution of the OI 5577 Å intensity. Notice the large peak centered between the 60° and 70° latitudes. Such a peak seem to arise from downward fluxes of energetic particles and it is called the "auroral maximum".

Fig. 24 shows the latitudinal location of the mid-latitude OI 5577 Å emission maxima for the European and American sectors. Notice the larger latitudinal variation for the American sector (bottom plot). Notice also that the plots of Fig. 24 do not include the auroral maxima.

More recently, Fukuyama (1977) carried out a statistical study on seasonal and long-term variations of

the nightglow emissions originated around the mesopause region. He related those nightglow variations to the upper atmospheric dynamics. He found that at low and mid latitudes the airglow seasonal variations consist of global fluctuations of quasibienial and 12-,6- and 4- month periods.

10. The Geocoronal Airglow

The earth's outer space is surrounded by hydrogen population that can emit airglow. The resulting airglow forms the geocoronal luminosity.

The hand-made sketch of Fig. 25 illustrates the spatial distribution of the Hydrogen Lyman α geocoronal airglow. The density of points in that figure is proportional to the hydrogen Lyman α intensity.

The geocoronal airglow is used to study the dynamics, chemistry and energy budgets of the Exosphere.

See references no. 21, 38, 39, 45, 59 and 77 for additional details on the geocoronal airglow features.

As explained in section 6.3 Kerr et al (1986) performed high resolution measurements of the geocoronal Balmer α emission, utilizing a Fabry-Perot interferometer located at Arecibo. Doppler line profiles permited to estimate exospheric temperatures.

Geocoronal photons permit the fluorescence of the geocoronal hydrogen ($3^2 P_{1/2} - 2^2 S_{1/2}$) which generates the 6563 Å airglow observed by Kerr et al (1986). Their airglow measurements permitted to study several thermodynamical and photochemical aspects of the exobase physics (for detail, see section 6.3).

Thomas and Madjas (1978) associated the Exospheric hydrogen abundance variations with the polar wind. Raideen et al (1986) showed geocoronal images obtained with the Dynamics Explorer (DE) satellite. Pursell and Tousey (1960) and Kupperian and Byram (1959) carried out rocket experiments on the H Ly α emissions. Emerick et al 1976 measured hydrogen densities and temperatures both in the dayside and in the nightside utilizing the geocoronal Ly airglow.

11. Ionospheric Studies Through Man-Made Airglow

11.1 Introduction

During the past few years ionospheric studies through man-made airglow has been getting increasing attention. The artificial or man-made airglow is obtained by means of chemical or dynamical modifications of the ionospheric plasma. Very often those experiments are concerned with studies of the ionospheric F-region.

The ionospheric modification, can be done in a large number of ways. It can be made through either chemical releases or through HF heating. In the former case, chemical elements such as SF_6, Ba, Sr, Eu, water etc. are used. In the second case high-powered HF radiowaves are utilized. Artificial airglow resulting from nuclear explosions have also been reported (Kofsky, 1967).

The ionospheric modification experiments have specific purposes. For instance, those ones using barium (Ba) and europium (Eu) clouds can be fitted to study the dynamical evolution of the ionospheric plasmas bubbles (see section 6.2). The Ba and Eu glow measurements permit to determine plasma velocities and instability processes.

Experiments utilizing water relases in the bottom edge of the F-region permit to study the ionospheric bubbles generation mechanisms. Ionospheric decreased electron concentration due to the water release cause decreases on the OI 6300 Å airglow that can be used to study the generation mechanism of the ionospheric plasma bubbles.

11.2 HF Heating Induced Airglow

It is well known that whenever sufficiently intense radiowaves at frequencies close to the F-layer

penetration frequency propagate in the ionosphere, the ionospheric plasma gets considerably modified. As a result, airglow alterations can be produced. Figure 26 illustrates the HF ray paths from ground to the reflection height for the ordinary and extraordinary components of the wave.

The HF heating can give rise to two opposite effects on the OI 6300 Å airglow intensity, depending on the amount of power used. When the HF power is relatively low, the predominant mechanism for the OI 6300 Å airglow alteration is through the chemical reactions envolved in the dissociative recombination production of the OI 6300 Å airglow. That is, HF raised electron temperatures decrease the dissociative recombination reaction rate which, in turn, result in decreased airglow emission. Therefore, the OI 6300 Å airglow tends to decrease with the HF heating.

The other effect, that is, OI 6300 Å airglow enhancements, occur when the HF power is high enough to produce OI 6300 Å airglow via electron impact excitation of oxygen a atoms.

Sobral (1978) utilizing the HF heating expriments at Arecibo calculated reaction rates of the chemical reactions involved in the production of OI 6300 Å via

dissociative recombination. Fig. 27 displays the red line enhencement caused by the suppression of HF power (see Sobral, 1978).

Biondi et al (1970) detected HF F-region electron heating through OI 6300 Å airglow measurements.

Fejer et al (1985) describes ionospheric heating experiments recently performed at Arecibo.

A very extensive literature on the ionospheric modification experiments utilizing the HF heating are given at the end of references list of the present manuscript. Such literature comes through two special issues of the Journal of Atmospheric and Terrestrial Physics, one of them in 1982 and the other one in 1985.

11.3 Chemical Release Induced Airglow

Haser (1967) carried out ionospheric electric field measurements utilizing barium cloud releases. The barium clouds velocities were measured from ground with the help of ground optical instrumentation.

Table 3 (source: Haser, 1967) shows a list of barium emission lines. Fig. 28 (source Haser, 1967) shows the spectral lines concerned with Ba vapor release.

Kofsky (1967) revised the airglow processes related with nuclear explosions. Table 4 (source: Kofsky, 1967)

shows a comparison between nuclear explosion induced lines and airglow emission obtained through other processes.

Bernhardt and Moore (1986) studied the excitation of oxigen permitted line emissions utilizing SF_6 cloud injections into the ionosphere. The sulfur hexafluoride (SF_6) has a high afinity to electrons and so, SF_6 releases tend to cause electron density holes in the ionosphere.

The SF_6 is one of the most extensively studied halogenated compounds for electron attachment (Bernhardt, 1986). The basic attachment reaction for the SF_6 is:

$$SF_6 + e \longrightarrow SF_6^- \qquad \text{rate:} \quad 10^{-9} cm^3/s$$

Theoretical calculations by Bernhardt et al (1986) have indicated that substantial airglow enhancements at λ = 8446 Å and 1356 Å is triggered by the SF_6 injection into the ionosphere.

12. The Dayglow

The dayglow or atmospheric emissions in the dayside of the earth has been used in studies of the neutral atmosphere composition and dynamics, and in the determination of ionospheric chemical reaction rates.

In general, the dayglow measurement techniques differ considerably from those utilized for nighttime measurements, in the sense that the dayglow measurements require the elimination of strong spurious airglow contamination that arises from the direct solar interaction with the earth's upper atmosphere.

Link et al (1983) presented a thorough analysis of dayglow emissions in the cleft region utilizing rocket measurements. The wavelengths analysed were the following: 4278 Å, 5200 Å, 5577 Å and 6300 Å. It is concluded that neutral winds introduce modifications in the spacial distribution of the 5200 Å and the 6300 Å airglow.

McCoy et al (1985) carried out remote sensing measurements of the ionospheric F_2 region utilizing dayglow emissions at λ = 834 Å. Neutral atmospheric composition and ionospheric density distributions were studied utilizing 834 A profiles variations.

In an earlier work, Noxon (1967) makes a comprehensive description of the dayglow. Torr et al (1986) studied the O_2 thermospheric dayglow.

Cleary (1986) observed at high latitude, dayglow emissions from NO molecules at the γ, δ and ε bands.

The use of weak band systems (0,1), (0,2) and (0,3) permit to determine NO densities between 105 Km and 125 Km.

Charkrabarti (1985) presented satellite EUV (300-900 Å) dayglow measurements taken in the polar cap. High-resolution EUV emission measurements help to study of the energetics and the morphology of such emissions. In particular, auroral emissions measurements below λ = 1000 Å can provide useful information on the excitation mechanism, photochemistry and energetic budget (Chakrabarti, 1985).

13. Perspective Optical Studies of the Ionosphere in the Near Future

The optical studies of the ionosphere through airglow techniques is gaining momentum at present.

Integrated international world-wide coordinated measurements are being urged by the international scientific community. An example of that is the effort proposed in 1984 by the Bureau of the SCOSTEP (Scientific Committee on Solar-Terrestrial Physics) to the SCOSTEP president, Professor K. D. Cole in which a global study of the ionosphere would be proposed. As a result a program called WITS (World Ionosphere/Thermosphere Study) was created.

The ionospheric optical measurements play a major role in such integrated global ionospheric experiments.

In fact, in the United States, a major prcgram for upper atmosphere research using ground-based optical techniques, namely, the CEDAR (Coupling, Energetics and Dynamics of Atmospheric Regions) group, has been established in 1986. Such a program has been formaly proposed by the Ground-Based Optical Aeronomy (GBCA) science steering committee (see CEDAR reference at the end of the reference list of this work).

The CEDAR program development in the next few years will follow according to three phases (Phases I, II and III).

Fig. 29 posts the major science topics during Phases I, II and III.

Fig. 30 shows the world-wide CEDAR program distribution of Fabry-Perot observing stations.

Fig. 31 shows CEDAR Program and Data Management.

Fig. 32 displays the world-wide distribution of optical observations that took part in the 1985/86 Mesopause OH nightglow intensity and temperature measurement program.

Fig. 33 displays the CEDAR management flow chart.

REFERENCES

1. Akasofu, S. I. and J. R. Kan, Editors", Physics of the Auroral Red Arc Formation". Geophysical Monograph 25, AGU Series 1981.

2. Anger, C. D., "Review of Rocket Auroral Measurements". Aurora and Airglow. Edited by Billy McCormac, Reinhold Publ. Corp., 1967.

3. Barbier, D., "Interpretation de la Luminescence Nocturne de la Raye Roge de l'Oygene". C. R. Acad. Sci. Paris 244, 2077-2080, 1957.

4. Barbier, D., "L'Activité Aurorale Aux Basses Latitudes". Ann. Geophys., 14, 334-335, 1958.

5. Bernhardt, P. A., E. J. Moore, J. Baumgardner and M. Mendillo, "Excitation of Oxygen Permitted Line Emissions by SF_6 Injection into the F-Region". J. Geophys. Res. 91, A8, 8937-8946, 1986.

6. Biondi, M. A., Sipler, D. P. and R. D. Hake Jr., "Optical (6300 A) Detection of Radiofrequency Heating of Electrons in the F-Region". J. Geophys. Res., 75, 6421-6424, 1970.

7. Blamont, J. E. and J. Barat, "Dynamical Structure of the Atmosphere Between 80 and 120Km".*

8. Bythrow, P. F., M. A. Doyle, T. A. Potemra, L. J. Zanetti, R. E. Huffman, C. I. Meng, D. A. Hardy, F. J. Rich and R. A. Heelis, "Multiple Auroral Arcs and Birkeland Currents: Evidence for Plasma Sheeet Boundary Waves". Geophys. Res. Lett. 13, no. 8, 805-808, 1986.

---

*Aurora and Airglow. Edited by Billy McCormac, Reinhold Publ. Corp., 1967.

9. Chakrabarti, S. "EUV (300-900A) Spectrum of Polar Cap and Cusp Emissions Near Local Noon". J. Geophys. Res. 90, A5, 4421-4426,1985.

10. Chakrabarti, S., "Extreme Far Ultraviolet Emissions from the Polar Cap". J. Geophys. Res. 91, A7, 8065-8072, 1986.

11. Chapman, Sydney, "History of Aurora and Airglow" Aurora and Airglow". Edited by Billy McCormack-Reinhold Publ. Corpor., 1967.

12. Clary, D. D., "Daytime High-Latitude Rocket Observations of the NO , and bands". J. Geophys. Res. 91, A10, 11337-11344, 1986.

13. Cogger, L. L., J. S. Murphree, C. A. Tepley and J. W. Meriwether Jr., ,"Measurements of E-Region Neutral Wind Field". Planet, Space Sci. 33, no. 4, 373-380, 1985.

14. Cogger, L. L., J. C. G. Walker, J. W. Merriwether Jr. and R. G. Burnside, "F-Region Airglow: Are Ground-Based Observations Consistent with Recent Satellite Results?". J. Geophys. Res. 85, A6, 3013-3020, 1980.

15. Cole, K. D., "Stable Auroral Red Arcs, Sinks of Energy for D_{st} Main Phase". J. Geophys. Res. 70, 1689, 1965.

16. Cornwall, J. M., F. V. Coroniti and R. M. Thorne, "Unified Theory of SAR Arc Formation at the Plasma Pause". J. Geophys. Res. 76, 4428-4445, 1971.

17. Craven, J. D., L. A. Frank and K. L. Ackerson, "Global Observations of a SAR Arc". Geophys. Res. Lett. 9, no. 9, 961-964, 1982.

18. Dandekar, B. S. and J. Turtle, "Atomic Oxygen Concentration from the Measurements of the OI 5577A Emission of the Airglow". Planet. Space Sci. 19, 949-957, 1971.

19. Daniell, R. E., D. J. Strickland, "Dependence of Auroral Middle UV Emissions on the Incident Electron Spectrum and Neutral Atmosphere". J. Geophys. Res. 91, A1, 321-327, 1986.

20. Esther, R. H. and D. L. Reasoner. "Spectrophotometry of Faint Light Sources With a Tilting Filter Photometer". Applied Optics 8, no. 2, 227-242, 1969.

21. Emerick, C., S. Cazas and J. E. Blamont, "Exobase Hydrogen Donsity and Temperature from Lyman Absorption and Polarization Measurements, 2, Dayside and Night Side Results During April 1971". J. Geo-Phys. Res. 81, 6103-6114, 1976.

22. Erdman, P. W. and E. C. Zipf, "Dissociative Excitation of the $N^+(^5S)$ State by Electron Impact on N_2: Excitation Function and Quenching". J. Geophys. Res. 91, A10, 11345-11351, 1986.

23. Feier, J. A., C. A. Gonzalez, H. M. Ierkic, M. P. Sulzer, C. A. Tepley, L. M. Duncan, F. T. Djuth, S. Ganguly and W. D. Gordon "Ionospheric Modification Experiments with The Arecibo Heating Facilities". J. Atmos. Terr. Phys. 47, no. A12, 1165-1179, 1985.

24. Fesen, C. G. and V. J. Abreu, "Modeling the 6300A Low Latitude Nightglow", J. Geophys. Res. 92, no. A2, 1231-1240, 1987.

25. Frank, L. A. and J. D. Craven, "Polar Views of the Earth's Aurora With Dynamics Explorer". Geophys. Res. Lett. 9, no. 9, 1001-1004, 1982.

26. Fukuyama, K., "Airglow Variations and Dynamics in the Lower Thermosphere and Upper Mesosphere-II Seasonal and Long Term Variations". J. Atmos. Terr. Phys. 39, no. 1, 1-15, 1977.

27. Gadsden, M. and E. Marovich, "5577A Nightglow and Atmospheric Movements". J. Atmos. Terr. Phys. 31, 817-825, 1969.

28. Gadsden, M., "Twilight Observations"*

29. Gerard, J. C. and C. E. Noel, "AE-D Measurements of the NO Geomagnetic Latitudinal Distribution and Contamination by the $N^+(^3S)$ Emission". J. Geophys. Res. 91, A9, 10136-10140, 1986.

30. Green, B. P., W. T. Rawlins, R. M. Nadel, "Diurnal Variability of Vibrationally Excited Mesospheric Ozone as Observed During the Spire Mission". J. Geophys. Res. 91, A1, 311-320, 1986.

31. Gulledge, I. and Packer, "High Altitude Profiles of the OI 5577A and 6300 A Night Airglow Layer Derived from Rocket Photometry". Astron. J., 163, 1966.

32. Hasegawa, A., K. Mima, "Anomalous Transport Produced by Kinetic Alfvén Wave Turbulence", J. Geophys. Res. 83, 1117, 1978.

33. Haser, L., "Use of Artificial Barium Clouds to Study Magnetic and Electric Fieldss in the Atmosphere". *

34. Hernández, G. J. and J. P. Turtle, "Kinetic Temperature Measurements of the 5577 A OI Line of the Night Airglow".*

35. Hernández, G., "Analytical Description of a Fabry Perot Interferometer". Appl. Optics 5, no. 11, 1745-1748, 1966.

36. Herrero, F. A. and J. W. Meriwether Jr., "Equatorial Nightime F-Region Events: A Survey of 6300 A Airglow Intensity Maps at Arecibo", J. Atmos. Terr. Phys. 43, no. 8, 859-866, 1981.

37. Hunter, D. M. and M. B. McElroy, "Quenching of Metastable States of Atomic and Molecular Oxygen and Nitrogen". Space Sci. Rev., 6, 493-573, 1967.

*Aurora and Airglow. Edited by Billy McCormac Reinhold Publ. Corp., 1967.

38. Ishimoto, M., M. R. Torr, P. G. Richards and D. G. Torr, "The Role of Energetic O^+ Precipitation in a Mid-Latitude Aurora". J. Geophys. Res. 91, A5, 5793-5892, 1986.

39. Kerr, R. B., S. K. Atreya, J. W. Meriwether Jr., C. A. Tepley and R. G. Burnside, "Simultaneous H Line Profile and Radar Measurements at Arecibo". J. Geophys. Res. 91, A4, 4491-4512, 1986.

40. Kileen, T. L. and P. B. Hays, "$O(^1S)$ from Dissociative Recombination of O^+_2 Nonthermal Line Profile Measurements from Dynamics Explorer". J. Geophys. Res. 88, 10163-10169, 1983.

41. King, J. W., H. Kohl and R. Pratt, "The Effect of Atmospheric Neutral Winds on the Height of the F_2-Layer Peak at Middle and High Latitudes". J. Atmos. Terr. Phys. 29, 1529-1539, 1967.

42. Kofsky, I. L., "Clarification of Airglow Processes by Nuclear Excitation".*

43. Kozyra, J. U., T. E. Cravens, A. F. Nagy, M. O. Chandler, L. H. Brace, N. C. Maynard, D. W. Slater, B. A. Emery and S. D. Shauhan, "Characteristics of Stable Auroral Red Arc Event". Geophys. Res. Lett. 9, no. 9, 973-976, 1982.

44. Kumar, S., S. Chakrabarti, F. Paresce and S. Bowger, "The O^+ 834A Dayglow Satellite Observations and Interpretation with a Radiation Transfer Model". J. Geophys. Res. 88, A11, 9271-9279, 1983.

45. Kupparian, J. E. Jr., E. T. Byrom, J. A. Chubb and H. Friedman, "Far Ultraviolet Radiation in the Night Sky". Planet. Space Sci., 3-6, 1959.

* Aurora and Airglow. Edited by Billy McCormac, Reinhold Publ. Corp., 1967.

46. Link, R., J. G. McConnel and G. G. Shepherd, "An Analysis of Spatial Distribution of Dayside Cleft Optical Emissions". J. Geophys. Res. 88, A12, 10145-10162, 1983.

47. McCoy, R. P., "Thermospheric Odd Nitrogen 1. NO $N(^4S)$ and $O(^3P)$ Densities from Rocket Measurements of the NO and Bands and the O_2 Herzberg J Bands". J. Geophys. Res. 88, A4, 3197-3205, 1983.

48. McCoy, R. P., D. E. Anderson Jr. and S. Chakrabarti", F_2 Region Ion Densities From Analysis of O^+834A Airglow: A Parametric Study and Comparisons with Satellite". J. Geophys. Res. 90, A12, 12257, 12264, 1985.

49. Meriwether, J. W. Jr., J. W. Moody, M. A. Biondi and R. G. Roble, "Optical Interferometric Measurements of Nighttime Equatorial Thermospheric Winds at Arequipa, Peru". J. Geophys. Res. 91, A5, 5557-5566, 1986.

50. Moor, J. G. and E. J. Weber, "OI 6300 A and 7774 A Airglow Measurements of Equatorial Plasma Depletions". J. Atmos. Terr. Phys. 43, no. 8, 851-858, 1981.

51. Myrabo, H. K., C. S. Deehr, C. J. Romick and K. Henriksen, "Midwinter Intensities of the Night Airglow O_2 (0-1) Atmospheric Band Emission at High Latitudes". J. Geophys. Res. 91, A2, 1690, 1986.

52. Nelson, G. Y. and L. L. Cogger, "Dynamical Behavior of the Nighttime Ionosphere at Arecibo". J. Atmos. Terr. Phys. 33, 1711-1726, 1971.

53. Noxon, J. F., "Dayglow Observations.*

*Aurora and Airglow. Edited by Billy McCormac, Reinhold Publ. Corp., 1967.

54. Peteherych, S., G. G. Shepherd and J. K. Walker, "Observation of Vertical E-Region Neutral Winds in Two Intense Auroral Arcs". Planet, Space Sci. 33 no. 12, 1985.

55. Peterson, V. L. T. E. Van Zandt and R. B. Norton, "F-Region Nightglow Emissions of Atomic Oxygen, 1. Theory". J. Geophys. Res. 71, 1715-1719, 1969.

56. Peterson, V. L., "F-Region Photochemical Nightglow Emissions".*

57. Peterson, V. L., T. E. Van Zandt and R. B. Norton, "F-Region Nightglow Emissions of Atomic Oxygen". J. Geophys. Res. 71, 2255-2265, 1968.

58. Pursell, J. D. and R. Tousey, "The Profile of Solar Lyman ". J. Geophys. Res. 65, 370-372, 1960.

59. Rairden, R. L., L. A. Frank and J. D. Graven, "Geocoronal Imaging with Dynamics Explorer". J. Geophys. Res. 91, A12, 13613-13630, 1986.

60. Rees, M. H., "Excitation of $O(^1S)$ and Emission of OI 5577 A Radiation in Aurora". Planet. Space Sci 32, 373, 1984.

61. Rees, M. H., and G. J. Romick, "Atomic Nitrogen in Aurora: Production, Chemistry and Optical Emissions". J. Geophys. Res. 90, A10, 9871-9879, 1985.

62. Richards, P. G. and D. G. Torr, "On the Production of N^+ by Energetic Electrons". J. Geophys. Res. 90, A10, 9917-9920, 1985.

*Aurora and Airglow. Edited by Billy McCormac, Reinhold Publ. Corp., 1967.

63. Rishbeth, H. and O. K. Garriott, "Introduction to Ionospheric Physics". Academic Press, N.Y., 1969.

64. Roach, F. E. and L. L. Smith, "The Worldwide Auroral Morphology".*

65. Sahai, Y., J. A. Bittencourt, N. R. Teixeira and H. Takahashi, "Plasma Irregularities in the Tropical F-Region Detected by OI 7774 A and 6300 A Nightglow Measurements". J. Geophys. Res. 86, A5, 3496-3500, 1981.

66. Sahai, Y. J. A. Bittencourt , N. R. Teixeira and H. Takahashi, "Simultaneous Observations of OI 7774 A and OI 6300 A Emissions and Correlative Study With Ionospheric Parameters". J. Geophys. Res. 86, A5, 3657-3660, 1981.

67. Shyn, T. W., S. Y. Pho and W. E. Sharp, "Differential Excitation Cross Section of Atomic Oxygen by Electron Impact: (^3P-^1S Transition)". J. Geophys. Res. 91, A2, 1986.

68. Sobral, J. H. A., "Medidas de Variacoes de Parametros de Atmosfera Neutra a partir de Medidas de Espalhamento Incoerente e de Luminescencia Noturna". Rev. Bras. Fis. 9, 473, 1979.

69. Sobral, J. H. A., H. C. Carlson, D. T. Farley and W. Swartz, "Nighttime Dynamics of the F-Region Near Arecibo as Mapped by Airglow Features". J. Geophys. Res. 83, 2561-2566, 1978.

70. Sobral, J. H. A., "Optical Measurements of the Quenching Coefficient of the O('D) State by Collisions With Ambient Molecules Utilizing the Ionospheric Heating Experiment". J. Atmos. Terr. Phys. 40, 945-948, 1978.

*Aurora and Airglow. Edited by Billy McCormac, Reinhold Publ. Corp., 1967.

71. Sobral, J. H. A., M. A. Abdu and I. S. Batista, Airglow Studies on the Ionosphere Dynamics over Low Latitude in Brazil". Ann. Geophys., t36, fasc. 2, 199-204, 1980.

72. Sobral J. H. A., "Association Between Plasma Bubble Irregularities and Airglow Disturbances over Brazilian Low Latitudes". Geophys. Res. Lett.,7, 980-982, 1980.

73. Sobral, J. H. A., M. A. Abdu, C. J. Zamlutti and I. S. Batista, "Wave Disturbances in the Low Latitude Ionospheric Plasma Depletions". J. Geophys. Res. 86, 1374-1378, 1981

74. Sobral, J. H. A., M. A. Abdu, Y. Sahai, "Equatorial Plasma Bubble Eastward Velocity Characteristics from scanning airglow photometers measurements over Cachoeira Paulista". J. Atmos. Terr. Phys., 47, nos. 8-10, 895-900, 1985.

75. Steiger, W. R., "Low Latitude Observations of Airglow".*

76. Thomas, L., "Ionospheric Implications of Aurora and Airglow Studies".*

77. Thomas, G. E. and A Vidal-Madjas, "Latitude Variations of Exospheric Hydrogen and the Polar Wind". Planet. Space Sci., 26, 873-882, 1978.

78. Tinsley, B. A., R. Rohrbaugh, H. Rassoud, Y. Sahai, N. Teixeira and D. Slater, "Low Latitude Aurorae and Storm Time Current Systems". J. Geophys. Res 91, A10, 11257-11269, 1986.

*Aurora and Airglow. Edited by Billy McCormac, Reinhold Publ. Corp., 1967.

79. Torr, M. R., B. Y. Welsh and D. G. Torr, "The O_2 Atmospheric Dayglow in the Thermosphere". J. Geophys. Res. 91, A4, 4561-4566, 1986.

80. Torr M. R. and D. G. Torr, "Energetic Oxygen in Mid-latitude Aurora". J. Geophys. Res. 89, 5547-5553, 1984.

81. Weber, E. J., J. Buchau, J. G. Moore, J. R. Sharber, R. C. Livington, J. D. Winningham and B. W. Reinisch, "F-Layer Ionization Patches in the Polar Cap". J. Geophys. Res. 89, A3, 1683-1694, 1984.

82. Weber, E. J., J. Aarons and A. L. Johnson, "Conjugate Studies of an Isolated Equatorial Irregularity Region". J. Geophys. Res. 88, A4, 3175-3180, 1983.

83. Weber, E. J., H. C. Brinton, J. Buchau and J. G. Moore, "Coordinate Airborne and Satellite Measurements of Equatorial Plasma Depletons". J. Geophys. Res. 87, no. A12, 10, 503,-10, 513, 1982.

84. Weill, G. M., "Airglow Observations Near the Equator".*

85. Wickwar, V. B., "Photoelectrons from the Magnetic Conjugate Point Studied by Means of the 6300 A Predawn Enhancement and Plasma Line Enhancement". Ph. D. Dissertation, Rice University, 1971.

SPECIAL ISSUES REFERENCES

J. Atmos., Terr. Phys. 44, no. 12, 1982. Special Issue on "Ionospheric Modification" with papers from the Twentieth General Assembly of the International Union of Radioscience.

J. Atmos. Terr. Phys. 47, no. 12, 1985. Special Issue on Active Experiments in Plasmas".

---

*Aurora and Airglow. Edited by Billy McCormac Reinhold Publ. Corp., 1967.

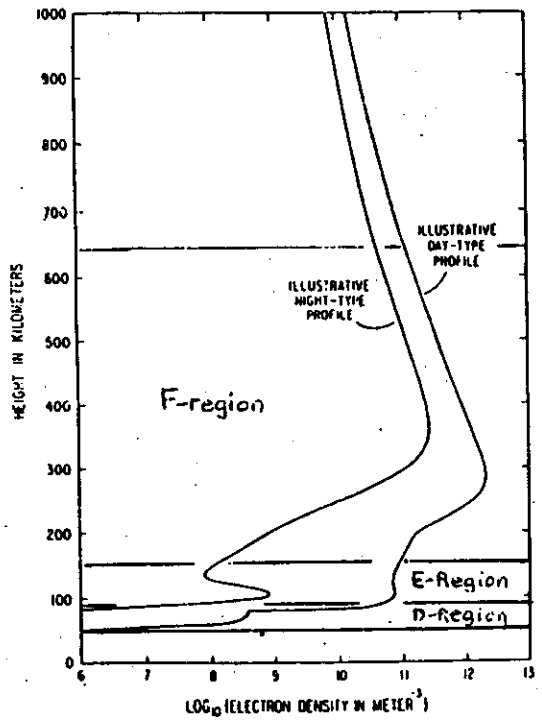

Source : E.P. Szuszczewicz (private communication)

Figure 1

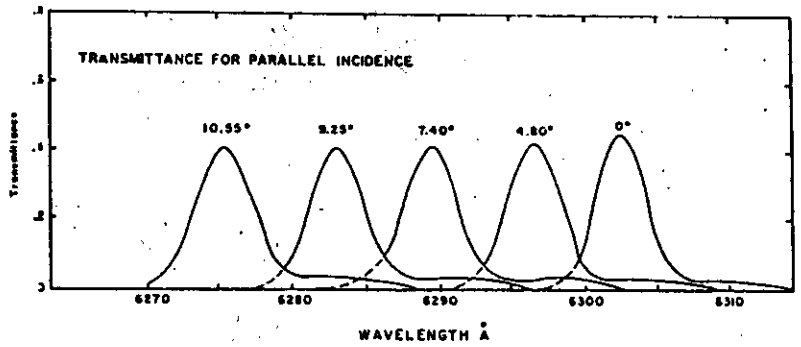

Figure 2

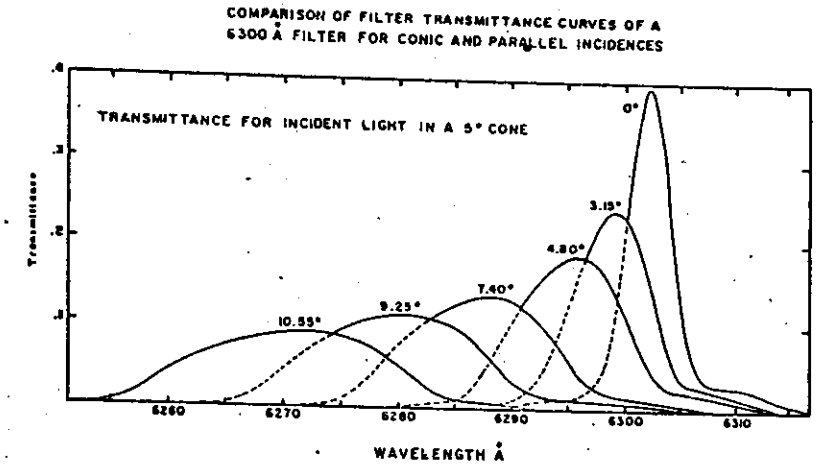

Figure 3

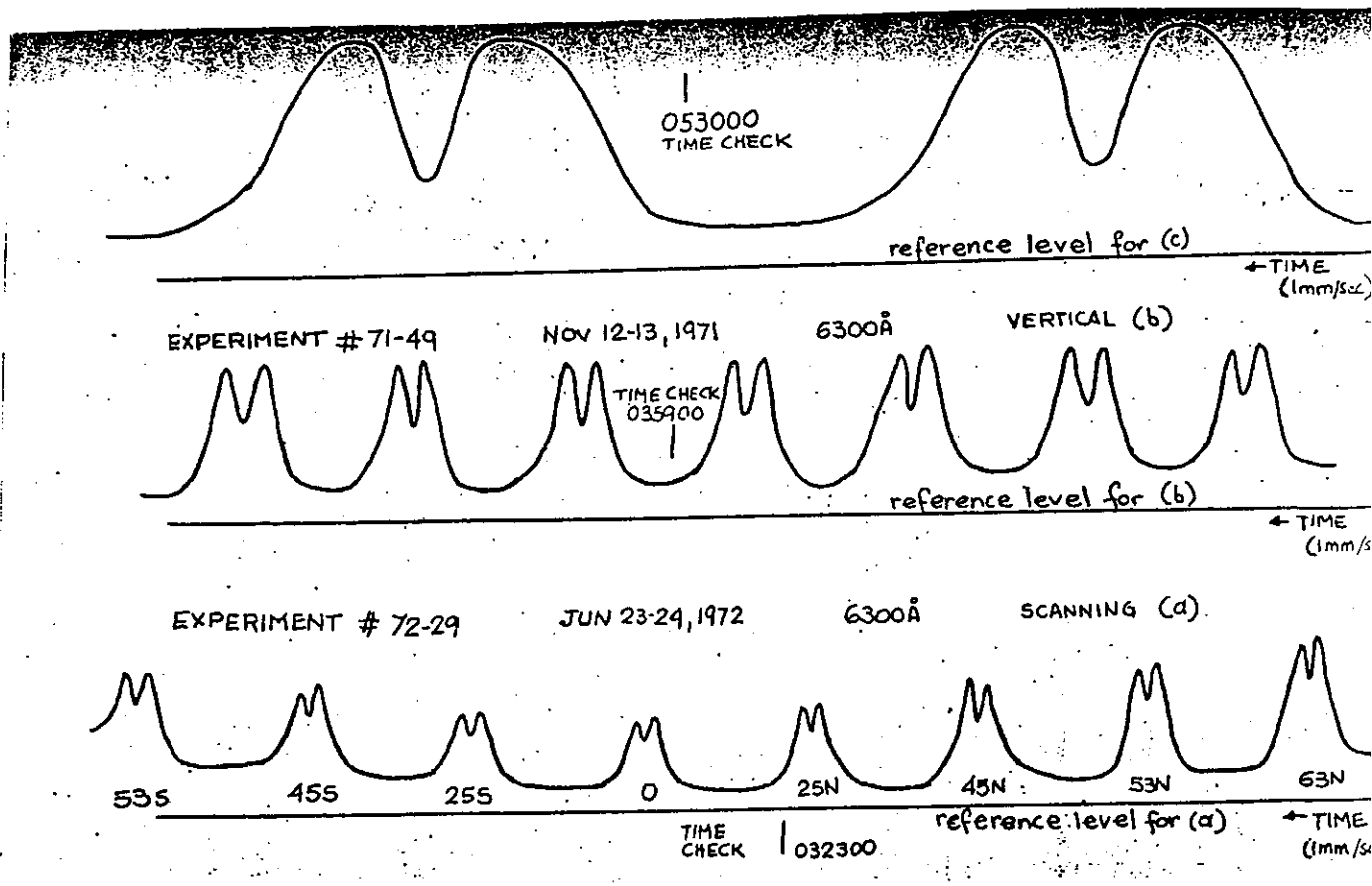

Figure 4

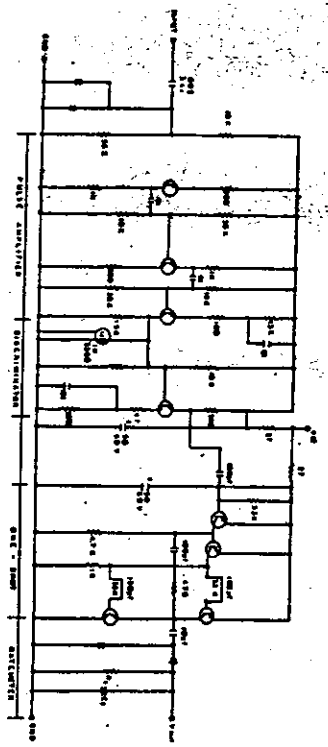

Figure 6

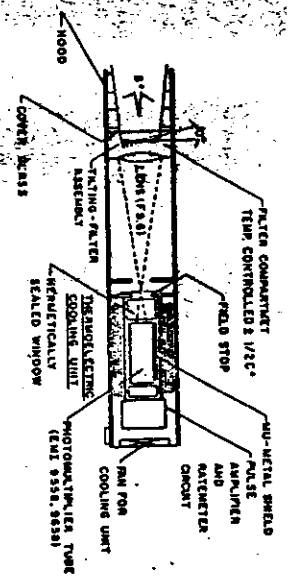

Figure 5

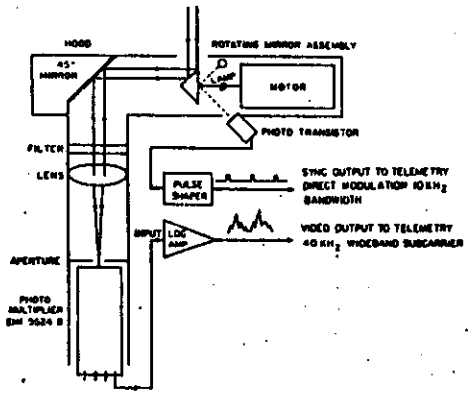

FIGURE 7. Schematic drawing of the auroral scanner, a device for producing high speed monochromatic pictures of the distribution of auroral luminosity over the sky around the rocket. More recent versions employ a dual filter housing mounted on the rotating mirror so as to provide alternate scans in 5577Å and 3914Å.

Source: Anger (1967)

Figure 7

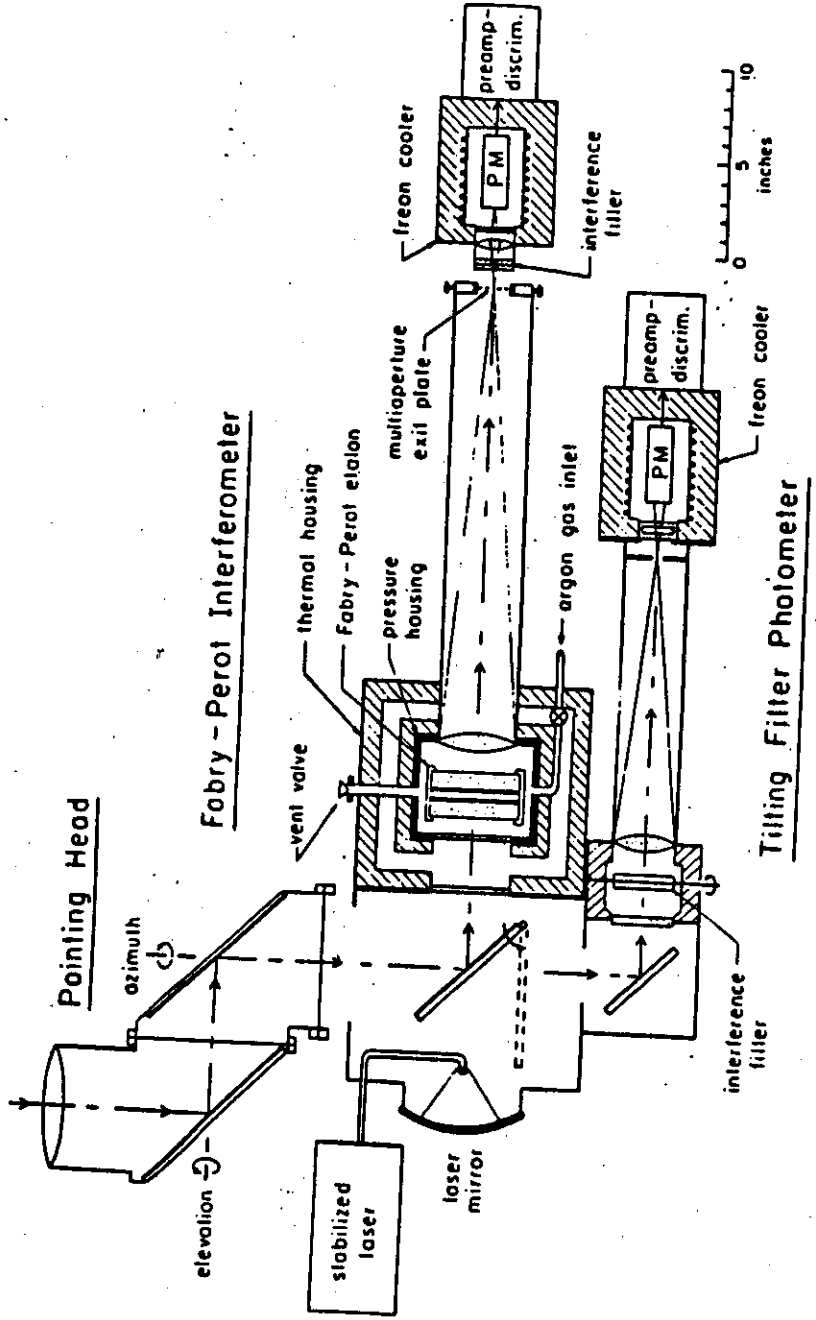

Source: Biondi (personal communication), 1987.

Figure 8

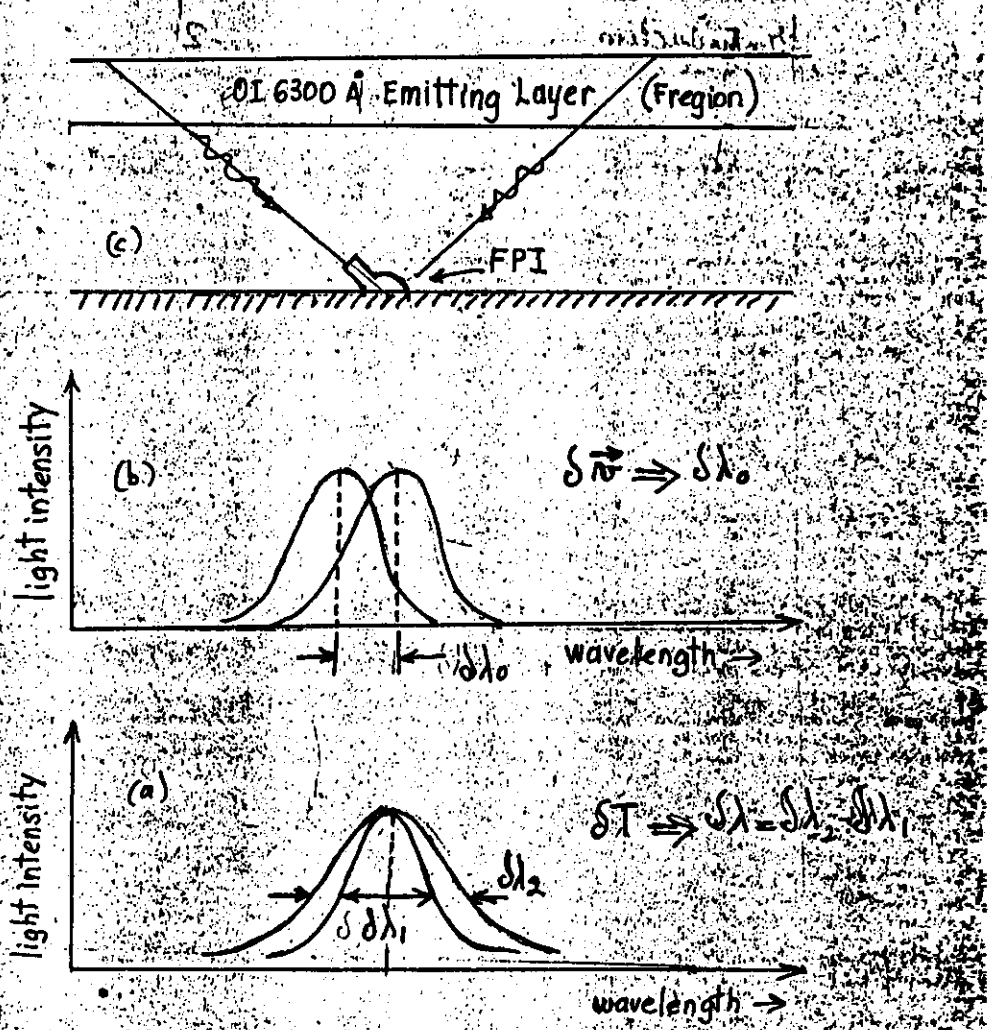

Figure 9

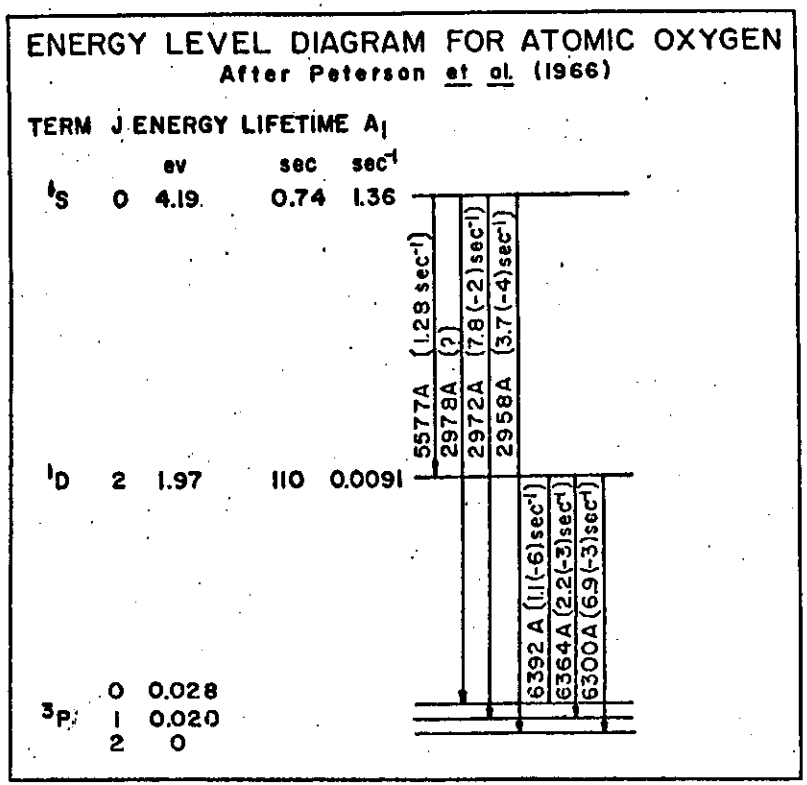

Figure 10

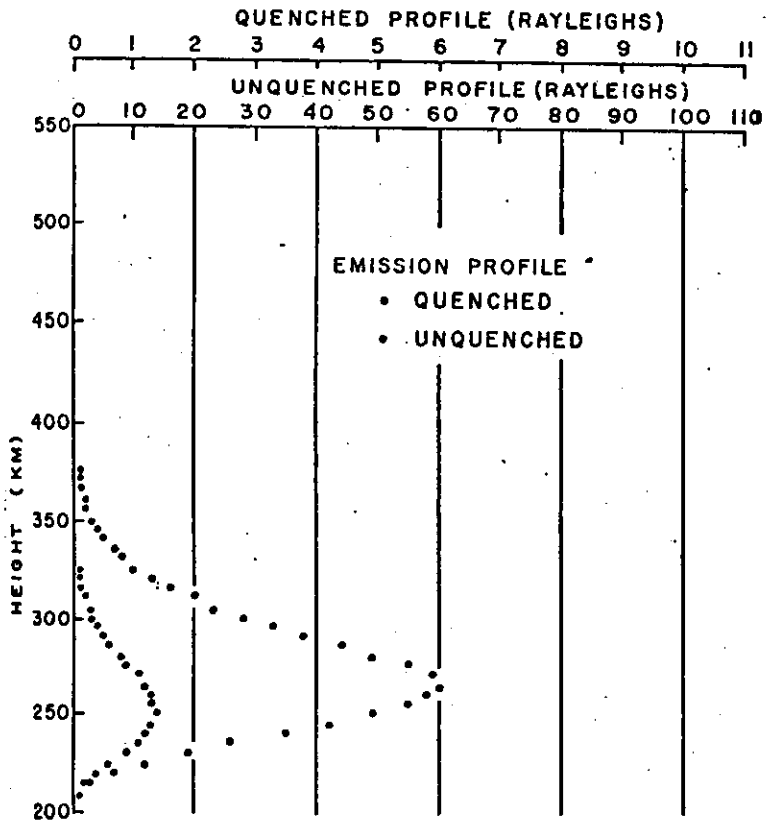

Figure 11

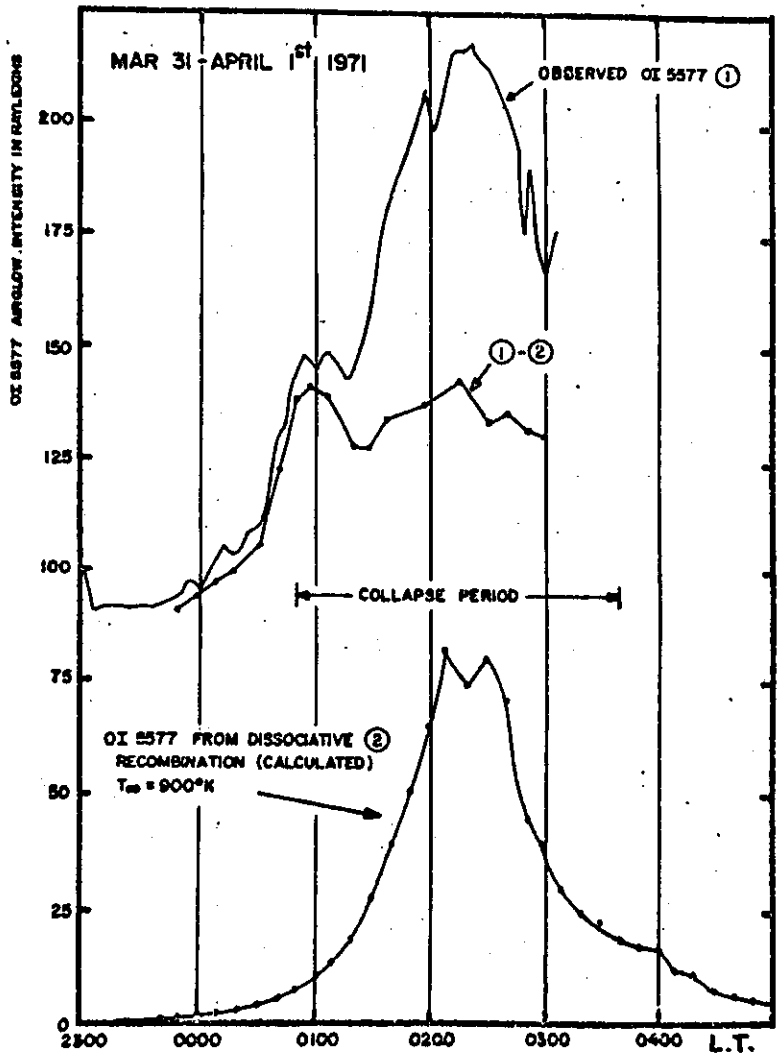

Figure 12

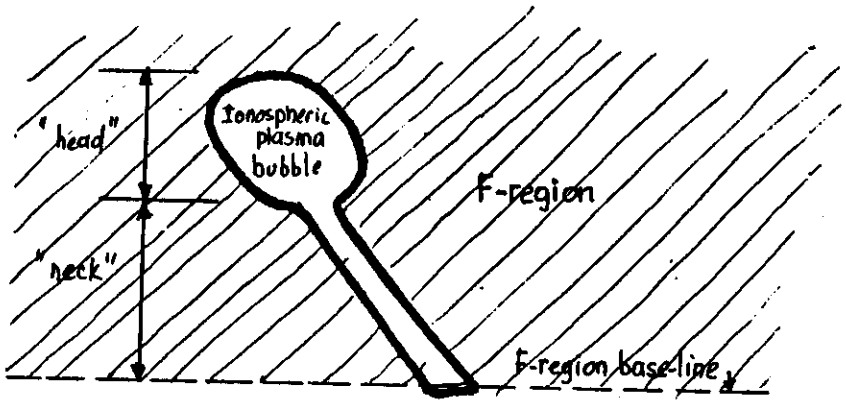

The shadded area indicates ionospheric plasma

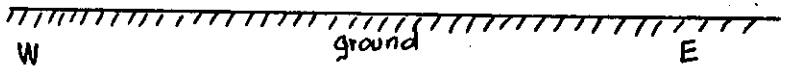

(a)

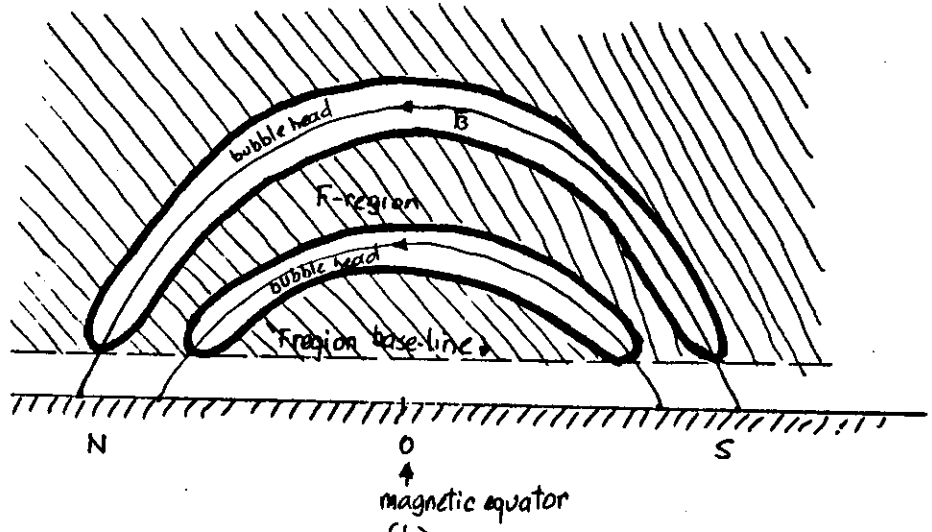

(b)

Figure 13

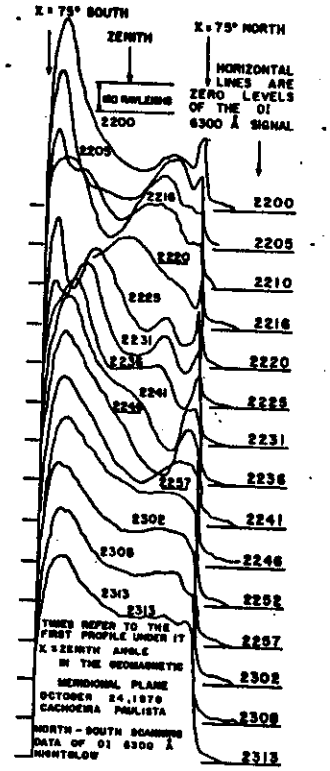

Fig. 2. Geomagnetic meridional profiles of the O I 6300-Å airglow intensity. A pronounced valley in the airglow profile appears at zenith at 2200 LT, which clearly propagates southwards. It corresponds to a large electron density rarefaction. Source: Sobral et al. 1981

Figure 14

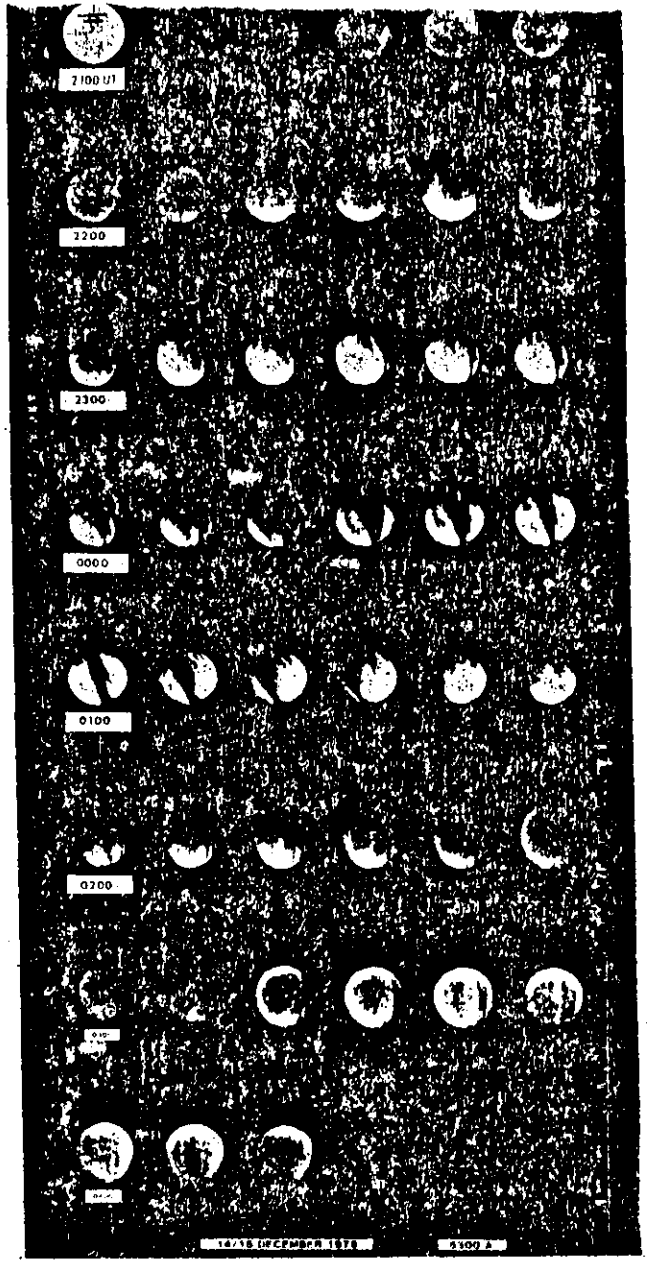

Fig. 3. All-sky (155° field of view) 6300-Å airglow images at 10-minute intervals for the flight of December 14–15, 1979.

Source : Weber et al. 1982

Figure 15

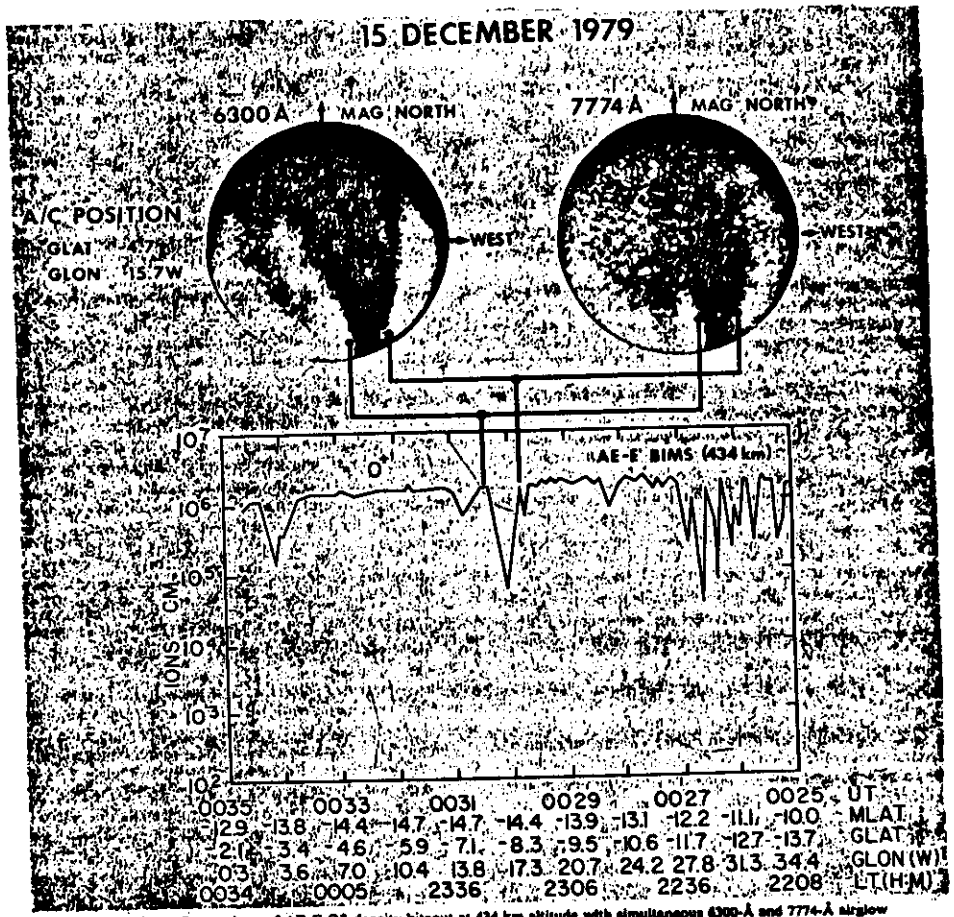

Fig. 5. Comparison of AE-E O+ density bitsout at 434 km altitude with simultaneous 6300-Å and 7774-Å airglow images. The edges of the O+ bitsout were mapped along magnetic field lines and projected into the 6300-Å image at 300 km and into the 7774-Å image at 360 km.

Source : Weber et al 1982

Figure 16

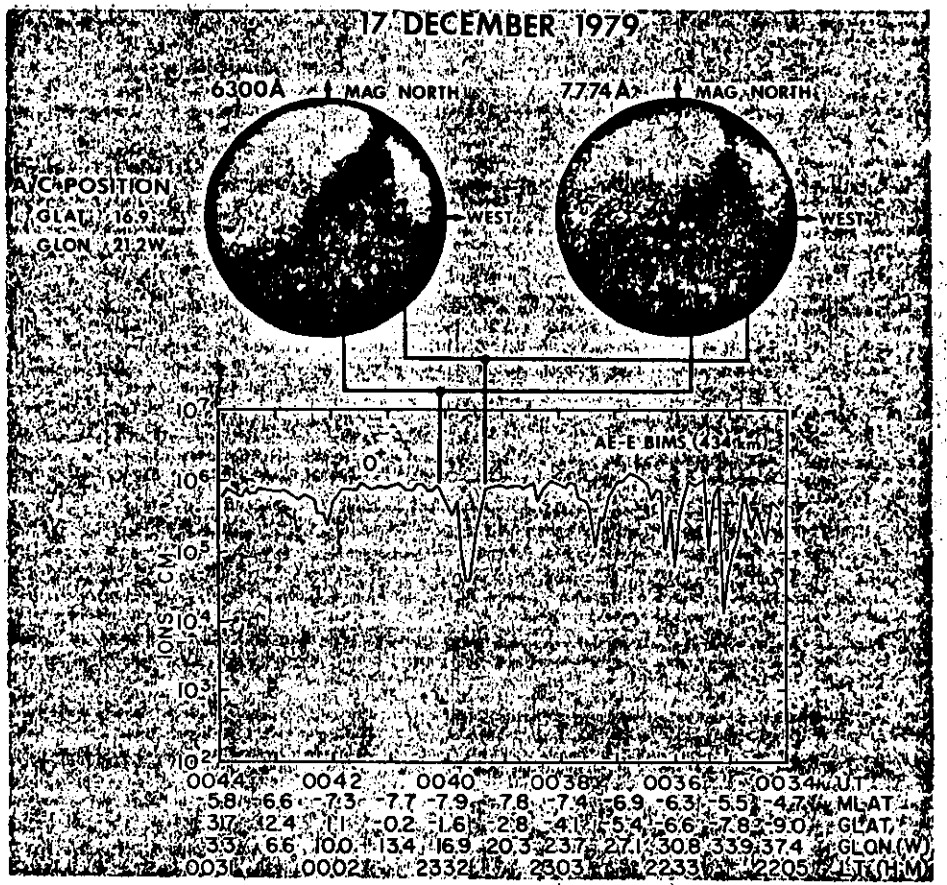

Fig. 9. Comparison of AE-E O+ bitcout measured at −8° MLAT at 0040 UT, December 17, 1979, with simultaneous 6300-Å and 7774-Å airglow images in the northern hemisphere. The edges of the O+ bitcout were traced along magnetic field lines and projected into the 6300-Å image at 300 km and into the 7774-Å image at 360 km.

Source: Weber et al. 1982

Figure 17

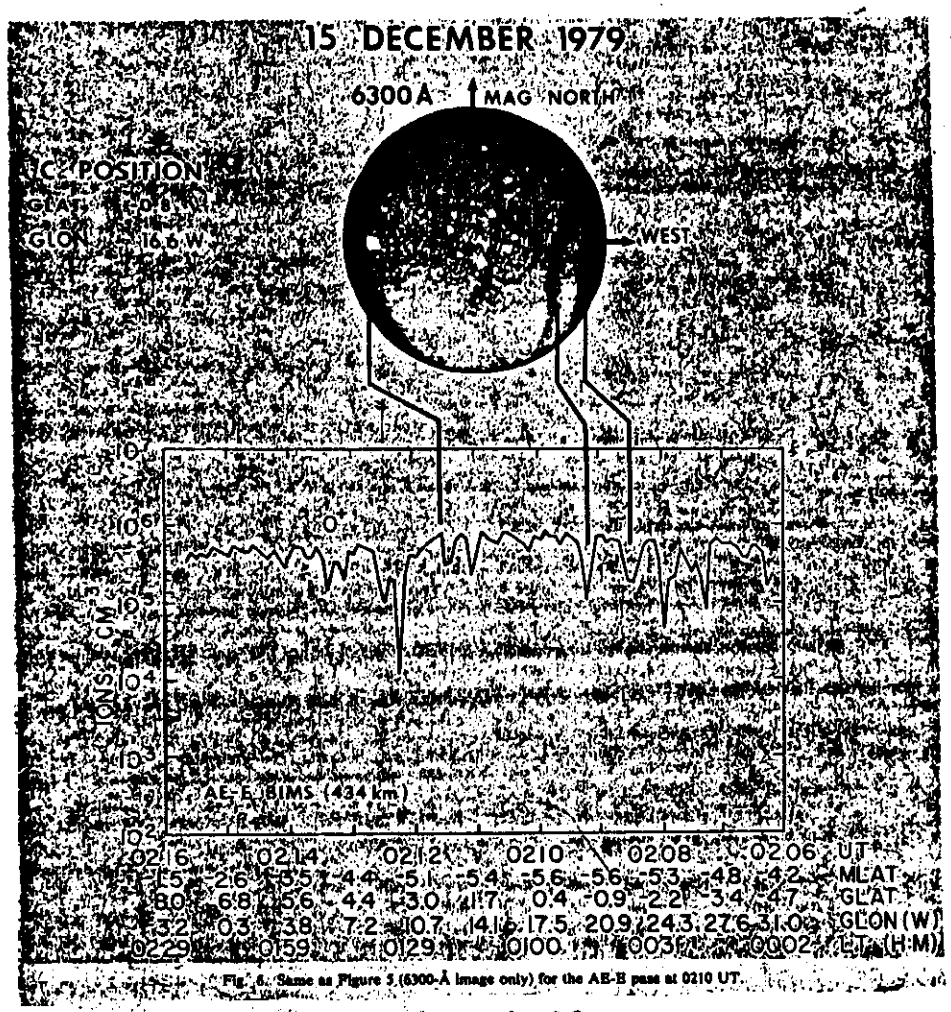

Fig. 6. Same as Figure 5 (6300-Å image only) for the AE-E pass at 0210 UT.

Source: Weber et al. 1982

Figure 18.

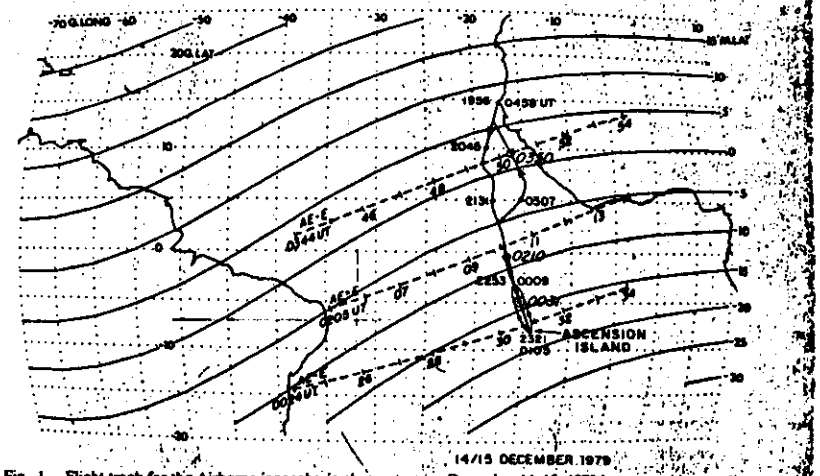

Fig. 1. Flight track for the Airborne ionospheric observatory on December 14–15, 1979 in geographic coordinates. Magnetic latitudes are also indicated. Subsatellite tracks for three successive AE-E passes are indicated at 1-minute intervals.

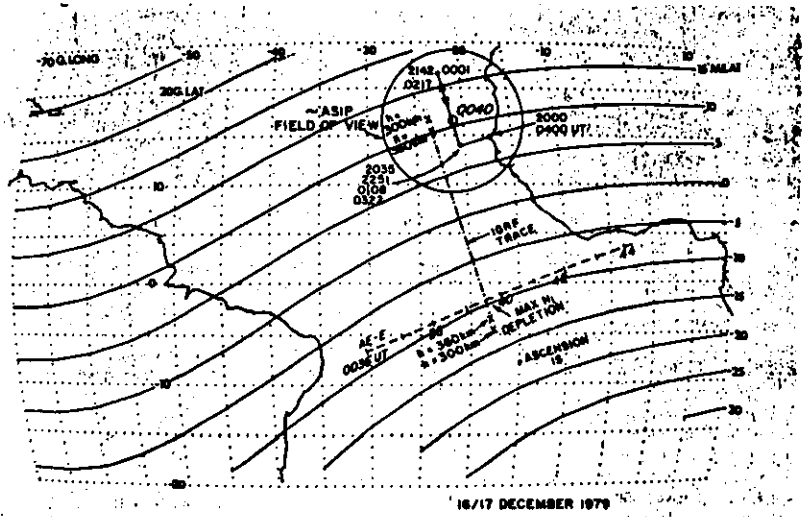

Fig. 8. Flight track for the AIO on December 1979 16–17, 1979 near the Ascension Island conjugate point. The AE-E subsatellite track for the pass at 0040 UT is shown at 1-minute intervals. The center of the large Ni depletion measured by the satellite at 434 km altitude and the north and south field line trace is also shown.

Figure 19

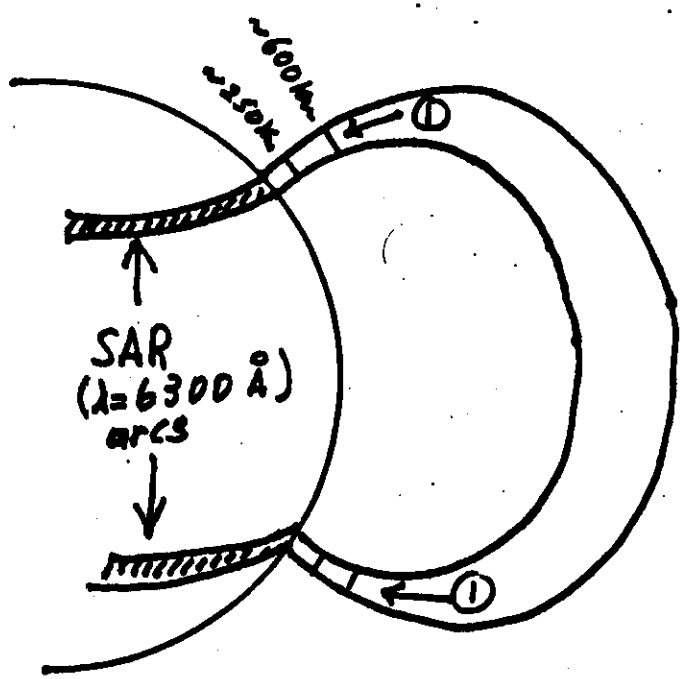

① downwards hot electrons flow

Figure 20

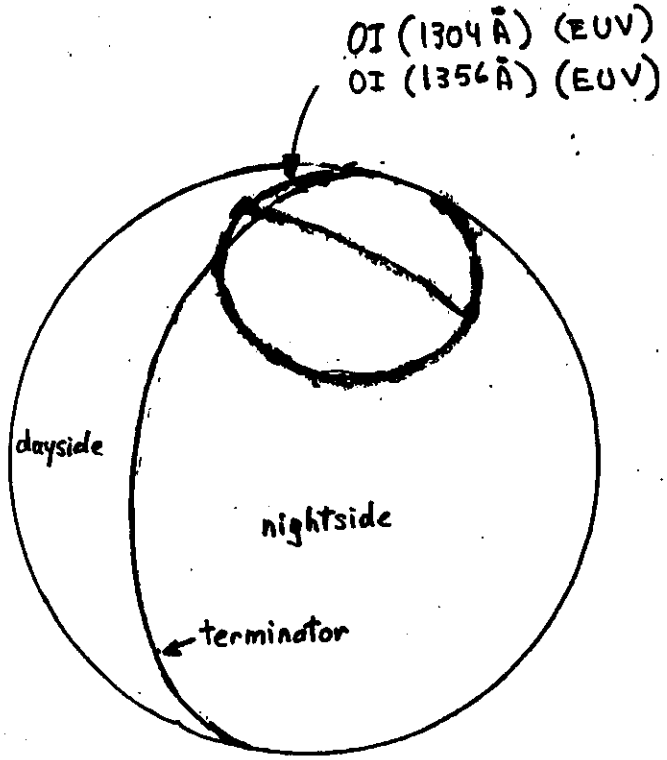

θ-shaped aurora (see real picture in Frank and Craven, 1982)

Figure 21

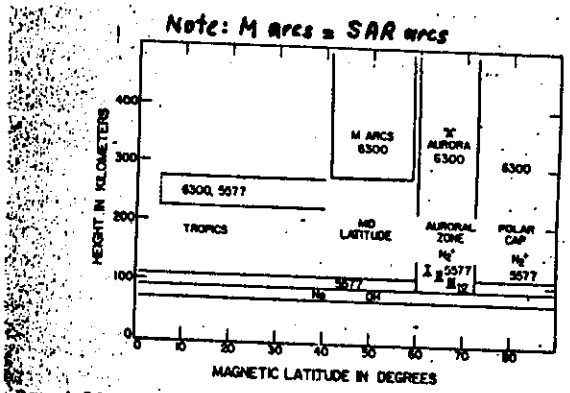

FIGURE 1. Schematic representation of upper atmosphere emissions as a function of height and latitude. The heights of auroras I, II, III, and IV are based on a recent study by HILLIARD and SHEPHERD (1966).

Source: Roach and Smith (1967)

Figure 22

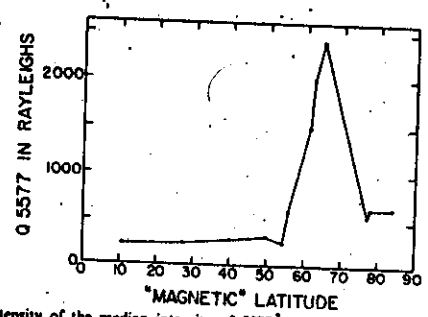

FIGURE 4. Intensity of the median intensity of 5577Å as a function of magnetic latitude.

source: Roach and Smith (1967)

Figure 23

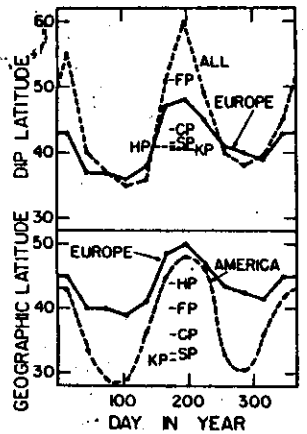

FIGURE 5. The latitudinal position of 5577Å maximum using the method of Glaume. Below: Results for Europe and for America as a function of geographic latitude. Above: Results for Europe and for "all" stations from Table X in GLAUME (1965).

*Results from Kitt Peak were not included in Glaume's analysis.

Source: Roach and Smith (1967)

Figure 24

Geocoronal Hydrogen Lyman-α* Intensity

* λ = 1216 Å

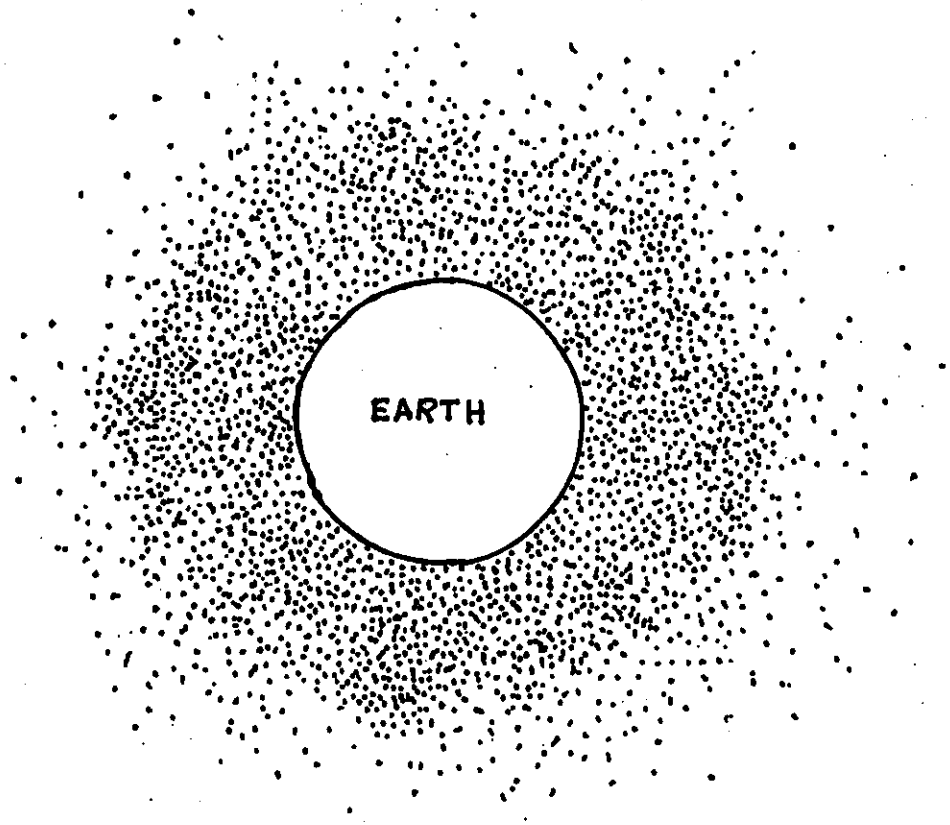

Figure 25

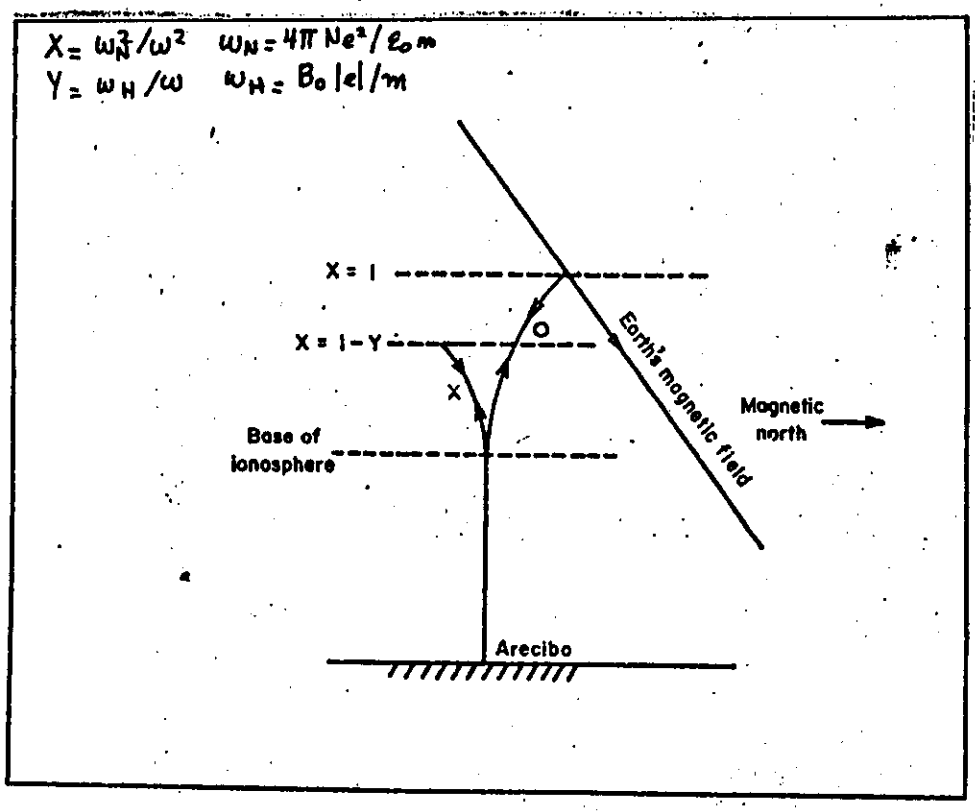

Figure 26

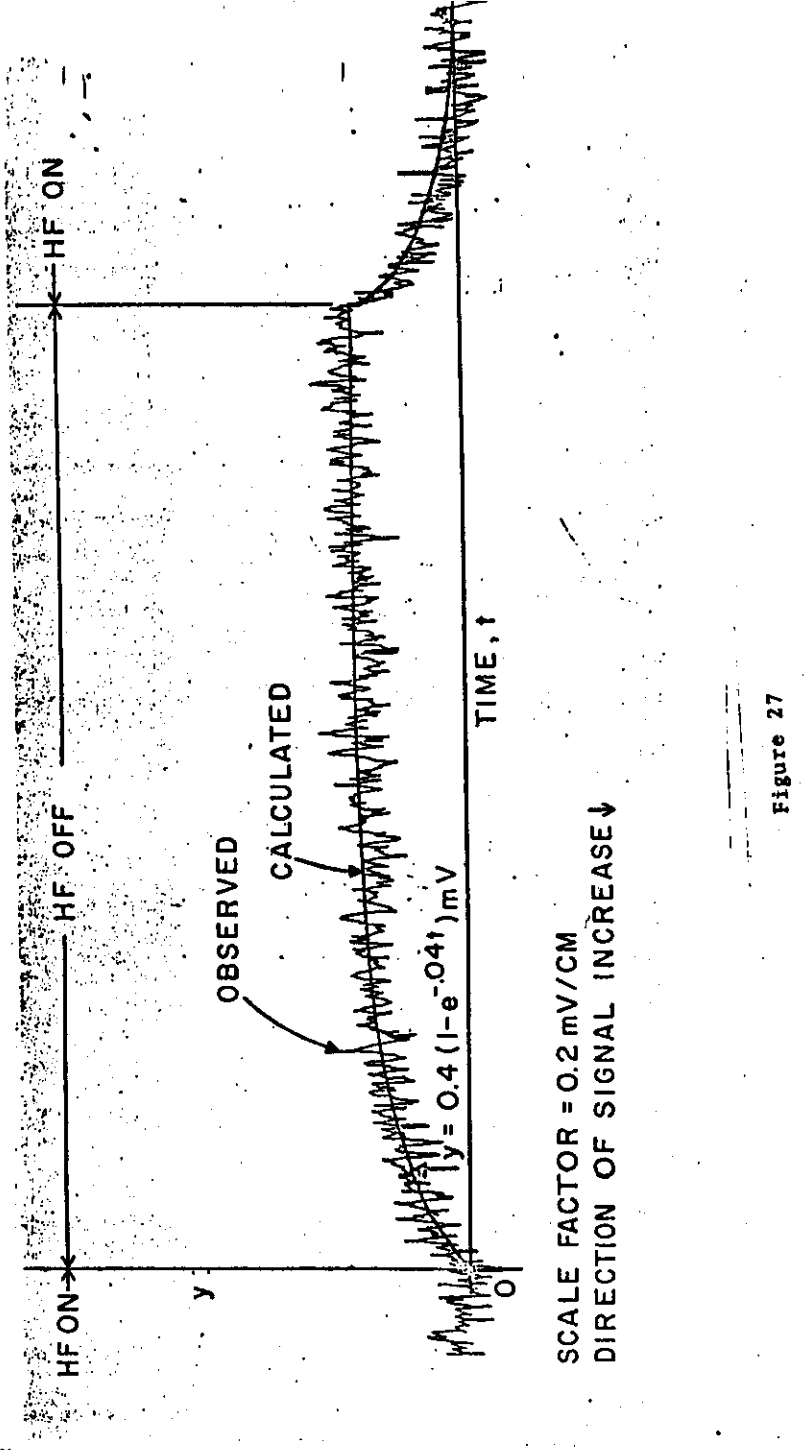

Figure 27

Spectra of Ba Clouds

Early spectral observations revealed only the resonance lines of the atoms present.

Ba I 5535,484Å $6s^2\ ^1S_0 - 6p\ ^1P_1^0$

Ba II 4934,088Å $6s\ ^2S_{1/2} - 6p\ ^2P_{1/2}^0$

4554,033Å $6s\ ^2S_{1/2} - 6p\ ^2P_{3/2}^0$

Sr I 4607,331Å $5s^2\ ^1S_0 - 5p\ ^1P_1^0$

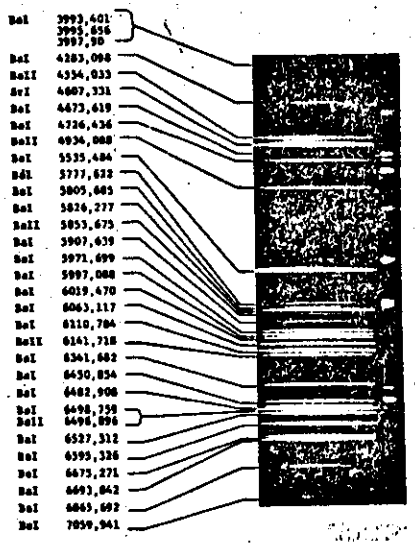

FIGURE 1. Spectrum of the initial phase of a Ba vapor release.

Source: Haser (1967)

Figure 28

MAJOR **CEDAR** SCIENCE TOPICS

PHASE I

Mean F-region global winds and temperatures, departures from mean
Auroral energy and momentum input, waves, perturbations
Equatorial, mid-latitude dynamics

PHASE II

Mean F-region global winds and temperatures, departures from mean
Detailed ion-neutral coupling
Auroral energy and momentum input, waves, perturbations
Dynamical effects of ring current particle precipitation
Exospheric hydrogen, line profiles, intensities
Metallic ions in mesosphere, layering, motion, abundances, temperatures
Auroral processes, atomic and molecular auroral spectroscopy
Lower thermosphere global dynamics
Latitudinal propagation of dynamical perturbations

PHASE III

Mean thermospheric composition, departures from mean, dynamical control
Lower thermosphere, mesosphere dynamics
E-region transport, dynamo effects, feedback to magnetosphere
Daytime thermospheric dynamics
Tides in the mesosphere and propagation to thermosphere
Gravity wave momentum, turbulence budgets
Ring current particle precipitation, global energetic consequences
Inter-hemispheric dynamical asymmetries, thermosphere and mesosphere
High-resolution studies of dynamics and composition, local features
Upper mesosphere, mesopause dynamics
Global distribution of exospheric hydrogen, quiet and disturbed conditions
Velocity distributions for exospheric helium
Thermosphere/Exosphere/Plasmasphere coupling
Thermosphere/Stratosphere coupling, minor constituent transport
Auroral morphology, physics and chemistry
Ozone and water vapor in the mesosphere, variability
Mesospheric eddy diffusion, height, seasonal variability
Metallic ion layering processes
Transition region active sounding
Mesospheric temperature structure
Dust, noctilucent cloud physics
Ionosphere/thermosphere feedback

FIGURE 3 1. "Growth curve" for CEDAR science during the three phases of the recommended program. A set of science topics related to the scientific goals of the Aeronomy Program is listed according to the phase of the CEDAR program for which the most rapid progress will be realized. The list is not all-inclusive, and many of the topics listed will be fruitfully studied at the times of other CEDAR phases. It illustrates, however, the accelerating rate at which important coordinated science can be done from the evolving network of coordinated CEDAR observatories.

Figure 29

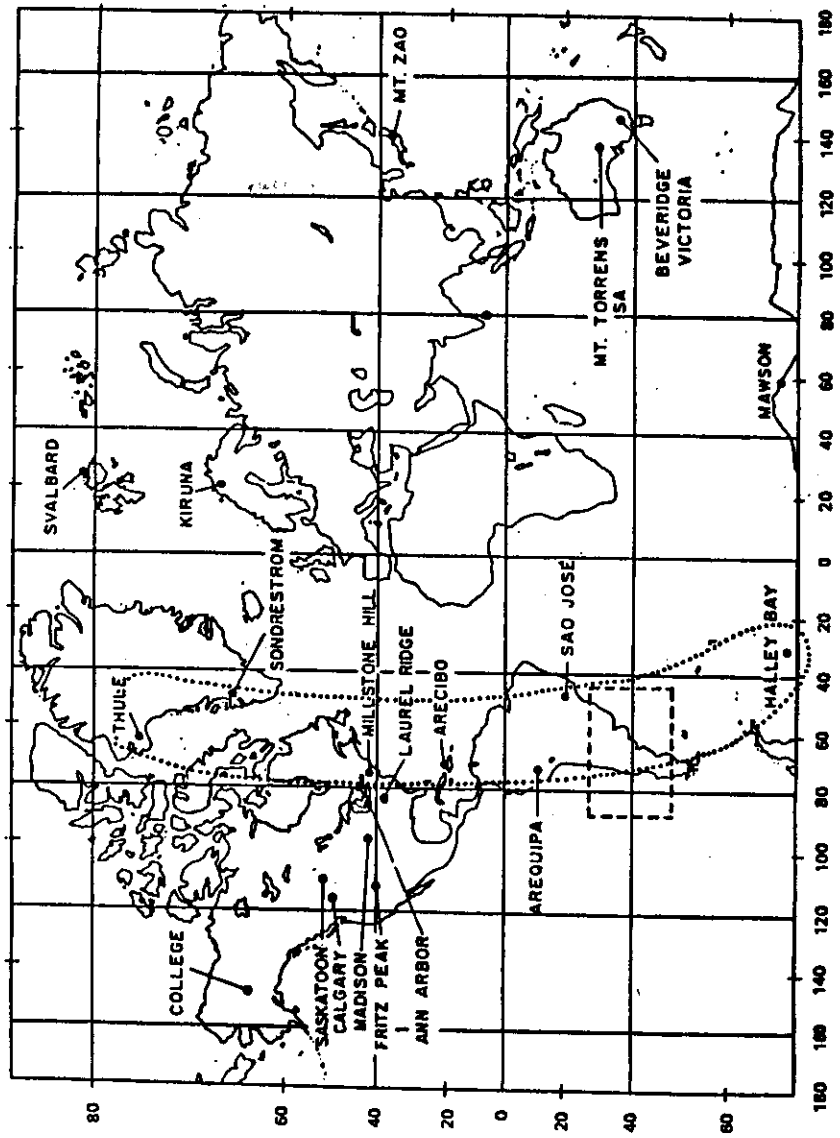

FIGURE 5.2 World-wide distribution of Fabry-Perot interferometer observatories, indicating present capabilities for coordinated measurements, as for example with the "pole-to-pole" longitudinal chain enclosed by the dotted line

Figure 30

PROGRAM AND DATA MANAGEMENT

CEDAR Steering Committee
Annual GBOA Workshops
NCAR Data Management Fellowships

PHASE I (1986–1987)

Image Plane Detector (IPD) evaluation and testing
Interferometer detector upgrades
Intensified monochromatic imager acquisition
Re-deployment of existing facilities

PHASE II (1988–1989)

Symposia and Data Workshops
Continued IPD evaluation and testing
Upgrade Rayleigh and resonance-scatter LIDARs (daytime operation)
Upgrade existing interferometers with IPDs
Increase number of intensified monochromatic imagers
Provide for station relocation and upgrade
Feasibility studies of Class I and very large aperture LIDAR
Design all imaging processing hardware and software for compatibility
Construct prototype: Visible region IPD spectrograph, Short IR WAMI, Long IR WAMI, WAMDII interferometer, Equatorial station Fabry-Perot interferometer and Class I imager.

PHASE III (1990–1992)

Symposia and data workshops
Construct Class I spectrometric, imaging and interferometric systems for the six key stations including multiple, simplified 1990 technology systems for broad station distribution and at least one Class I LIDAR
Upgrade existing LIDAR systems
Add additional etalons to existing Fabry-Perot interferometers
Enhance theoretical modeling and data analysis capabilities
Establish management, maintenance, and repair program for facilities and key stations

FIGURE 4.1 Evolutionary development of instrumentation and facilities for the CEDAR program. The time line is a conceptual estimate.

Figure 31

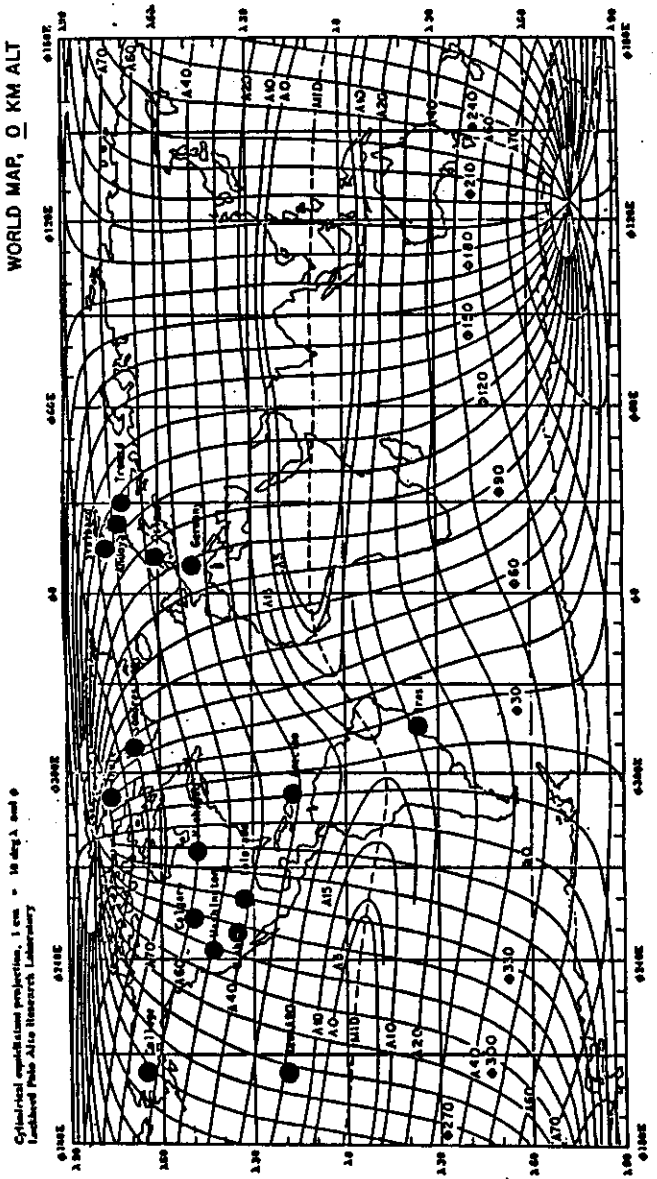

FIGURE 4.2 Optical observatories taking part in the 1985/86 Mesopause OH intensity and temperature measurement program.

Figure 32

NATIONAL SCIENCE FOUNDATION
DIVISION OF ATMOSPHERIC SCIENCE

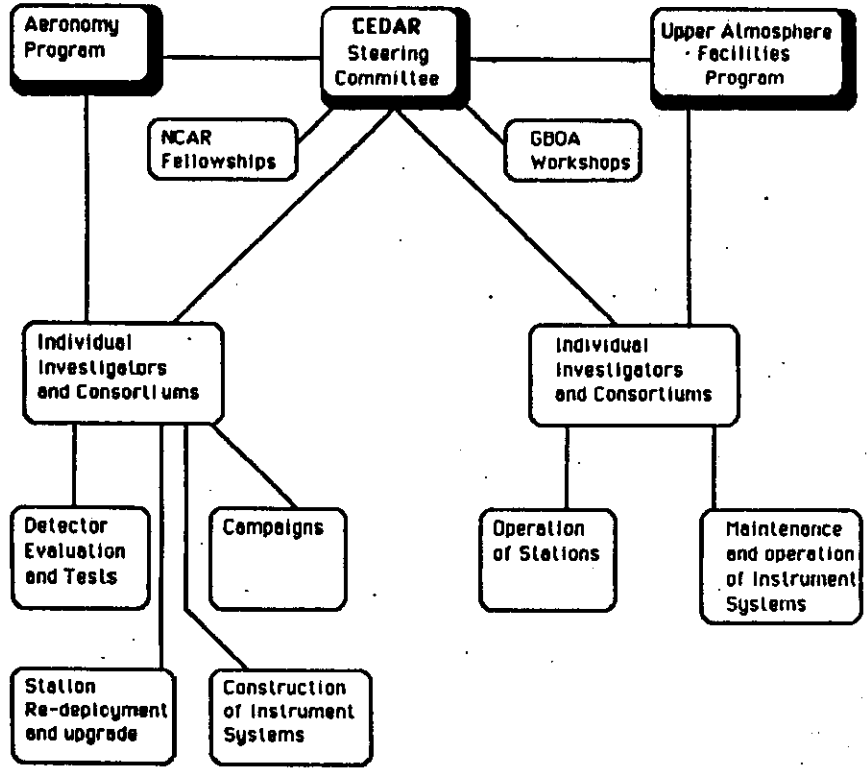

FIGURE 4.3 Facility Management Flow Chart.

Figure 33

Spectral Features Observed in Low-Latitude Aurorae

Feature	λ,A	Excitation Potential, ev
Atomic lines		
[N I] $^2D^o$–$^4S^o$	5198–5201	2.37
[N I] $^4p^o$–$^2D^o$	10,395–10,404	3.56
[O I] ^1D – ^3P	6300	1.96
[O I] ^1S – ^1D	5577	4.17
[N II] ^1S–^1D	5755	18.57
[O II] ^2P–^2D	7319–7330	18.61
N I 3^4P^o–3^4P	8216	11.79
N I 3^4D^o–3^4P	8680	11.71
O I 5^3D^o–3^3P	5958	12.97
O I 4^3D^o–3^3P	6157	12.70
O I 3^3P– 3^3S^o	7774	10.69
O I 3^3P–3^3S^o	8446	10.94
O I 3^3D–3^3P	9266	12.05
O II 3^2D^o–3^2P	4416	26.14
H Balpha 3^2D–2^2p^o	6563	12.04
H Balpha 4^2D–2^2P^o	4861	12.69
He I 2^3P^o–2^3S	10,830	18.83 (twilight)
He II Lyα 2^2D–1^2P^o	304	40.76
He II Paα 4^2D–3^2P	4686	
Molecular Bands		
N_2 + 1N		15.5 (twilight) 18.7 (night)
N_2+ Meinel		16.7
$N_2$1 P ?(weak)		7.3

TABLE 1

TABLE 1. Downlooking Intensities of Spectral Features

Feature	Nightside Aurora A	Airglow B	Polar Cap C	Sunlit Cusp D
OII 834	126.4	38.2	22.9	231.3
NII 916	23.6	–	–	83.6
NI 953 N_2	30.8	–	14.2	65.8
OI 989 N_2 985	153.6	44.1	149.1	1091.0
OI 1027 HI 1025	199.5	36.9	22.7	132.3
NII 1085 N_2 1083	178.3	26.9	≤ 5	294.6
NI 1134	79.0	11.6	20.2	255.6
NI 1168 HeI 584x2	116.1	23.2	32.3	97.2
HI 1216 NI 1200	6352.8	5705.9	6533.3	14025.7
NI 1243	90.0	7.3	–	125.4
N_2 1273	30.9	–	–	59.5
OI 1304 N_2 1298	1061.2	237.5	715.2	5107.1
N_2 1325	37.9	–	≤ 30	67.8
OI 1356 N_2 1354	285.2	66.6	118.1	577.3

values are in rayleighs

Source: Chakrabarti, 1986

TABLE 2

Table I. Spectral Data

λ cloud (Å)	Int.	Emitter	Transition	λ Lab. (Å)
3995	1	Ba I	$5d\,^3D_3 - 4f\,^3F_4^\circ$	3993,401
			$- 4f\,^3F_3^\circ$	3995,656
			$- 4f\,^3F_2^\circ$	3997,90
4284	2	Ba I	$5d\,^1D_2 - 4f\,^1F_3^\circ$	4283,098
4554	5	Ba II	$6s\,^2S_{1/2} - 6p\,^2P_{3/2}^\circ$	4554,033
4608	10dd	Sr I	$5s^2\,^1S_0 - 5p\,^1P_1^\circ$	4607,331
4675	1	Ba I	$5d\,^3D_3 - 7p\,^3P_2^\circ$	4673,619
4726	6	Ba I	$5d\,^1D_2 - 7p\,^1P_1^\circ$	4726,436
4934	6	Ba II	$6s\,^2S_{1/2} - 6p\,^2P_{1/2}^\circ$	4934,088
5535	10dd	Ba I	$6s^2\,^1S_0 - 6p\,^1P_1^\circ$	5535,484
5778	3	Ba I	$6p\,^3P_2^\circ - 6d\,^3D_3$	5777,622
5806	3	Ba I	$5d\,^3D_3 - 6p'\,^3F_3^\circ$	5805,685
5826	10d	Ba I	$5d\,^1D_2 - 6p'\,^1P_1^\circ$	5826,277
5854	1	Ba II	$5d\,^2D_{3/2} - 6p\,^2P_{3/2}^\circ$	5853,675
5908	3	Ba I	$5d\,^3D_1 - 6p'\,^3P_2^\circ$	5907,639
5971	10d	Ba I	$5d\,^3D_3 - 6p'\,^3P_2^\circ$	5971,699
5997	10d	Ba I	$5d\,^3D_1 - 6p'\,^3P_1^\circ$	5997,088
6019	10d	Ba I	$5d\,^3D_1 - 6p'\,^3P_0^\circ$	6019,470
6063	10dd	Ba I	$5d\,^3D_2 - 6p'\,^3P_1^\circ$	6063,117
6111	10dd	Ba I	$5d\,^3D_3 - 6p'\,^3P_2^\circ$	6110,784
6142	8	Ba II	$5d\,^2D_{3/2} - 6p\,^2P_{3/2}^\circ$	6141,718
6342	9	Ba I	$5d\,^3D_3 - 6p'\,^3D_3^\circ$	6341,682
6451	9	Ba I	$5d\,^3D_1 - 6p'\,^3D_2^\circ$	6450,854
6483	8	Ba I	$5d\,^3D_2 - 6p'\,^3F_3^\circ$	6482,908
6498	10dd	Ba I	$5d\,^3D_3 - 6p'\,^3D_3^\circ$	6498,759
		Ba II	$5d\,^2D_{3/2} - 6p\,^2P_{1/2}^\circ$	6496,896
6527	10d	Ba I	$5d\,^3D_2 - 6p'\,^3D_2^\circ$	6527,312
6595	10d	Ba I	$5d\,^3D_1 - 6p'\,^3D_1^\circ$	6595,326
6675	10	Ba I	$5d\,^3D_3 - 6p'\,^3D_1^\circ$	6675,271
6693	10	Ba I	$5d\,^3D_3 - 6p'\,^3D_2^\circ$	6693,842
6866	2	Ba I	$5d\,^1D_2 - 6p'\,^3P_2^\circ$	6865,692
7060	1	Ba I	$5d\,^3D_3 - 6p'\,^3F_4^\circ$	7059,941

d = overexposed

λ Lab taken from Russell and Moore, 1955

Source: Haser, 1967

TABLE 3

Table I. Comparison of the Spectra of the Continuum Glows

Glow	Short-Wavelength Cutoff	Wavelength of Peak Intensity	Half Power Wavelengths	Infrared Emission
Nuclear (ionization) induced	<3950Å	5500–6000Å	≈4200– ≈6500Å	Several times stronger than visible; decreases beyond 1.6μ
Intense natural night sky* (including astronomical component and perhaps Herzberg bands)	≪4000Å	6200Å	4350–6750Å	
Normal natural night sky† (including astronomical component)	(≈4000Å**)	5700–5900Å	–6500Å	
Chemical release of NO; prompt and afterglow††	<3850Å	5000–5400Å	4600–6000Å	
Chemical release of NO; prompt glow***	≪4200Å	Subsidiary at 5800Å, then an increase to beyond 6400Å	5300– Å	
Laboratory NO + O††† (at ≈1 mm pressure; all others in this table at ≈10^{-4} mm)	3975Å	6000Å	4800–8300Å	Extends beyond 2μ, but intensity/μ much less than in the visible****

TABLE 4